Applied Energy 377 (2025) 124523

Contents lists available at ScienceDirect

Applied Energy

journal homepage: www.elsevier.com/locate/apenergy

Design and operation of future low-voltage community microgrids: An AI-based approach with real case study

Md Morshed Alam [a], M.J. Hossain [a,*], Muhammad Ahsan Zamee [a], Ahmed Al-Durra [b]

[a] School of Electrical and Data Engineering, University of Technology Sydney, Ultimo, 2007, NSW, Australia
[b] Department of Electrical Engineering & Computer Science, Khalifa University, Abu Dhabi, United Arab Emirates

GRAPHICAL ABSTRACT

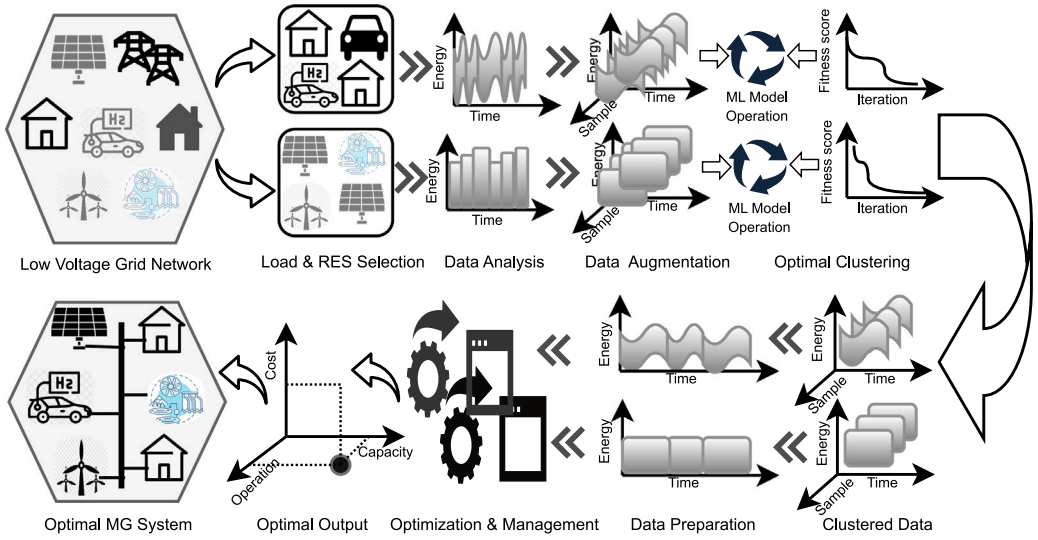

ARTICLE INFO

Keywords:
Microgrid
Energy management system
Artificial intelligence
Clustering algorithm
MILP optimization
PSO optimization
Hydrogen-based electrical vehicle

ABSTRACT

The utilization of artificial intelligence in the design and operation of a microgrid (MG) can contribute to improve its energy efficiency, resiliency, and cost of energy supply. This research proposes a new approach to conduct a comprehensive analysis for transforming existing low-voltage networks into MGs to achieve the net-zero goal by 2050. A data-driven machine learning-based clustering and profiling approach is designed and implemented to extract the data, constraints, and dependencies from the historical data. Furthermore, the constraints and dependencies are utilized for determining the renewable energy sources' capacity. A Bi-level optimization technique is developed to ensure appropriate coordination of cost and renewable energy source (RES) capacity. A comprehensive analysis is carried out utilizing real historical demand and generation data of an energy community in Australia. Based on the clustered analysis, the consecutive day's data are considered for the analysis. The findings reveal that the proposed microgrids achieve higher renewable RES utilization and lower electricity costs compared to grid-connected systems, with the potential to reduce carbon emissions by up to 98.23% when transitioning from coal-based grid systems to the proposed microgrid system. Additionally, a transformation from a grid time-of-use tariff-based system to the proposed microgrid setup can lead to a cost

* Corresponding author.
E-mail address: jahangir.hossain@uts.edu.au (M.J. Hossain).

https://doi.org/10.1016/j.apenergy.2024.124523
Received 24 March 2024; Received in revised form 28 June 2024; Accepted 15 September 2024
Available online 2 October 2024

reduction of 65.45%. These case studies will also assist the researcher in identifying new, potential ideas and industries to accelerate the implementation of remote community microgrids.

1. Introduction

The development of a renewable energy sources (RESs)-based microgrid (MG) for a remote community is an effective way to reduce energy costs and carbon emissions. Taking advantage of modern technology such as artificial intelligence (AI) and hybrid optimization, the transformation of MGs with the integration of RES is one of the appropriate candidates to improve the reliability of the present energy system. The integration of RESs into the grid offers multiple benefits, such as decreasing dependence on fossil fuels, enhancing RES usage, lowering energy production costs, reducing greenhouse gas emissions, and enhancing power quality.

In the realm of MG transformation, researchers have explored two primary avenues. Firstly, attention has been directed towards transitioning from traditional energy communities to RES-based MG systems. Alternatively, another focus area involves converting various energy systems into MG structures. Notably, a limited number of studies, such as those conducted by Zhou et al. [1] and Bin et al. [2], delve into the transformation of MGs from existing energy communities, emphasizing the consideration of crucial parameters and interdependencies. Conversely, a predominant proportion of research efforts concentrate on the transformation of MG systems from any energy system through sizing and design aspects. Researchers have dedicated their investigations to this facet, concentrating on the integration of RES, battery energy storage systems (BESS), and fuel cells (FC) [3,4]. Akter et al. [5] investigate off-grid power systems powered entirely by RES, considering various combinations of RES technologies. The objective of this research is to achieve optimal sizing for the MG. However, the focus has been primarily on daily average and annual demand, rather than employing a multifaceted, cluster-based, data-driven analysis.

The RES units can be incorporated into the energy system either individually or in combination. Studies in [6,7] combine different types of RESs, like photovoltaic (PV) and wind turbine (WT) systems, for the development and design of MG systems. A BESS is utilized as a storage solution, accounting for random demand and generation profiles without conducting a thorough analysis of demand and generation profiles. Ref. [8] includes multiple generation profiles for PV modules; however, it only takes into account the average demand and generation profiles. In addition, Guru et al. utilized random energy demand and PV generation profiles to ascertain the capacity of RES using a peak load shaving approach [9]. Furthermore, the optimal sizing of PV-BESS systems is determined using analytical methods that rely on comprehensive data on PV production and energy prices, as outlined in [10]. Out of the existing studies, none have opted for mini hydro (mHydro) as a RES. On the other hand, only Khezri et al. took into account the energy demand of electric vehicles (EV) when determining the optimal size for a home MG [11]. However, these studies have not incorporated AI-based, data-driven methodologies.

Several studies have been conducted using historical data and making appropriate assumptions regarding the system. Refs. [2,12] applied historical data without analyzing it or validating the obtained results across operational days. Meanwhile, Khezri et al. presented results for five operational days, yet the methodology for selecting these days is not described [11]. A multi-objective optimization strategy was employed to determine the optimal PV and WT capacity, focusing on minimizing the levelized cost and reducing the probability of power supply interruptions. The authors analyzed various combinations of autonomy days, leveraging historical data for this purpose [13]. Similarly, an approach grounded in electricity market dynamics was adopted for the optimal dimensioning of RES, with historical data informing the decision-making process [14]. A cost-centric framework was devised for standalone MGs to pinpoint the optimal size of PV and BESS using an analytical and economic sizing model [15]. In those scenarios, the analysis was conducted using historical data without engaging in any clustering or detailed profiling of demand and RES generation patterns. Conversely, the proposed model utilizes machine learning algorithms to cluster historical data into distinct days, enhancing the system's efficiency in data analysis and application.

However, Refs. [16,17] employed seasonal trend analysis for determining the optimal size of RESs in the MGs. Bacha et al. leveraged historical data alongside seasonal variations to ascertain the optimal capacity of RES, aiming to minimize expenses in remote rural regions and evaluated three distinct scenarios [18]. This approach limits the ability to acquire a comprehensive understanding of energy demand and RES generation patterns within the MG. Additionally, a selection of random, average, or standard day data [19,20] was used for analysis. This approach limits the ability to derive varied scenarios for energy communities from the data. The availability of RESs and the rise in demand within these communities remain unexplored. Thus, the sizing of RESs and storage systems is optimized only for specific scenarios, not for the system as a whole. Conversely, Refs. [4] and [21] implemented machine learning techniques, specifically k-means and k-medoids clustering, to achieve optimal sizing of RESs in off-grid MGs and on-grid households, respectively. These studies, however, overlook the potential integration of available RESs with the emerging demand, constrained by household and MG limitations. A recent study introduced clustering algorithms using self-organizing maps and fuzzy c-means to classify and generate consumption patterns [22]. A case study is conducted for optimal resident MG configuration through the integration of RES, diesel generator, and storage system [23]. In both cases, the authors applied HOMER software for sizing the MG rather than applying an advanced optimization algorithm.

The transformation of the MG from the existing energy system involves both capacity and operation adjustments. However, the majority of studies predominantly concentrate on identifying optimal capacities, often overlooking the optimization of energy flow and operation by employing linear programming (LP) and mixed-integer linear programming (MILP) optimization algorithms. For instance, Refs. [17] and [24] explored the use of metaheuristic algorithms like particle swarm optimization (PSO) and genetic algorithms (GA) for optimal sizing. By using a modified bio-inspired optimization algorithm and original PSO, the authors in [25] design a WT/hydrogen hybrid MG system with eight alternative small horizontal-axis WTs and investigate the effect of integration. Similarly, Mewafy et al. propose an optimized design approach for multi-use hybrid MGs by using a one-layer technique implemented with PSO to minimize costs and maximize reliability based on hourly data intervals [26]. Moreover, a one-layer deterministic mixed-integer nonlinear programming model is utilized for the optimal equipment selection, design, and scheduling of a power-to-gas integrated MG [27]. The impact of shared BESSs on load demand patterns in commercial-residential MGs, focusing on optimizing load demand patterns using peak-to-average ratio and demand profile smoothness is investigated to enhance performance and efficiency [28]. For sizing and optimizing the RES, Tatar et al. proposes a multiperiod two-stage stochastic MILP model by considering environmental uncertainty and carbon emission constraints [29]. However, the research field of sizing and optimizing RESs and storage systems for MGs and smart houses is extensive and continuously evolving. To provide context and comparison for the proposed study, the most relevant and recent studies in this area are compiled in Table 1. This table serves as a critical reference point, allowing readers to compare the methodologies, findings, and innovations of the proposed research with the existing studies in the field.

Nomenclature

α	optimization factor
β	binary variable
η	efficiency
γ	interest rate
$\hat{E}_D^{Com}$	Energy demand
$\hat{H}_D^{FV}$	H_2 demand
$\mathbb{C}$	cost
$\mathbb{Y}$	life time in year
H	set of house
ρ	water density
σ	discount rate
ξ	on/off status
A	area
CE	carbon emission
CEF	carbon emission factor
COE	cost of energy
d	day
E_G^{mH}	mhydro power generation
E_G^{PV}	PV power generation
E_G^{W}	WT power generation
g	acceleration
hi	height
i	set of index
j	interval
N	set of natural number
NPC	net present cost
o_c	optimal number of cluster
opt	optimal
r	rated/rate
s	interval in terms time unit
SOH	state of hydrogen
T	set of time
t	time
T_{hr}	set of time in hour
T_{mnt}	set of time in minute
T_{snd}	set of time in second
v	water speed
w	wind speed
c	cluster
Cap	capacity
cc	capital cost
ch	charge
ci	cut in
co	cut out
Com	Community
CoSA	Cooperation search algorithm
CSA	Chameleon swarm algorithm
D	demand
dc	discharge
EI	energy intensity
els	electrolyzer
ex	export energy
f	flat tariff
FV	Fuel cell electric vehicle
G	generation
HSH	hydrogen storage hub
im	import energy
M	number of module
mc	maintenance cost
mg	microgrid
mH	mini-Hydro
MOO	multi-objective optimization
mp	medium-peak
NMPC	Nonlinear model predictive control
op	off-peak
p	production
pk	peak
rc	replacement cost
RES	renewable energy sources
rf	refueling
SOC	state of charge
ST	storage tank
std	standard
sur	surplus of energy
TF	tariff
th	threshold
ToU	time of use
VMO	Vectorial microgrid optimization
WD	water discharge

The literature review indicates that most research primarily concentrates on the sizing of RESs and energy storage systems based on single-day scenarios or variable load and RESs generation profiles. There is a general neglect of considering historical data analysis on demand and generation for optimal sizing. The selection of demand and RESs generation patterns throughout the year is not adequately addressed. Researchers often focus on individual, random daily instances of PV generation and consumption profiles rather than examining multiple scenarios. This approach has left the impact of daily load and generation profile variability on cost–benefit analysis largely unexplored. The lack of long-term historical data on demand and generation reduces the precision and reliability of the MG operation and cost-benefit analyses. Therefore, the optimal sizing determined by these studies is confined to the specific demand and generation profiles they analyze, without encompassing the entire year.

To address these challenges, an AI-based data-driven approach is introduced, which enables us to comprehensively explore the actual benefits. The proposed system combines a machine learning-based clustering and profiling (MLCP) approach with a PSO-MILP-based bi-level optimization technique. This integration is specifically designed to optimize both the capacity and operation of low-voltage community MG. The novelty lies in the synergistic use of advanced machine learning techniques for data processing and state-of-the-art optimization methods to address the specific challenges of future community MG. Detailed mathematical models are formulated to support the MLCP algorithm and optimization technique. The MLCP algorithm utilizes K-means clustering along with a data distribution technique to realistically represent complex patterns in weather and energy usage over extended periods. This approach is not merely a replication of existing clustering techniques; instead, it extends their application by integrating them with complex optimization frameworks to address a very specific problem set. Additionally, a cost–benefit analysis and a carbon emission assessment on a real community MG is conducted. This evaluation not only demonstrates the practical applicability of the proposed system but also quantitatively measures its performance, providing a clear benchmark against existing solutions. The key contributions are the following:

Table 1
Overview of shortcomings in the existing studies (See [30]).

Ref.	RES			Storage		Demand		Analysis				Approach	
	mHydro	PV	WT	BESS	H_2/FC	Load	FCEV	Real data	Clustering	Sizing	Operation	OA	AI
[1]	×	✓	✓	✓	✓	✓	×	✓	×	✓	×	CSA	N/A
[3]	×	✓	✓	✓	✓	✓	×	×	×	✓	×	PSO-GA	N/A
[5]	×	✓	×	✓	✓	✓	×	✓	×	✓	×	MILP	N/A
[30]	×	✓	×	✓	×	✓	×	×	×	✓	×	NMPC	N/A
[8]	×	✓	×	✓	×	✓	×	×	×	×	✓	PSO	N/A
[7]	×	✓	✓	✓	×	✓	×	×	×	✓	×	N/A	N/A
[9]	×	✓	×	✓	×	✓	×	×	×	✓	×	CoSA	N/A
[6]	×	✓	✓	✓	×	✓	×	✓	×	✓	×	LP	N/A
[2]	×	✓	×	✓	×	✓	×	✓	×	✓	×	MILP	N/A
[16]	×	✓	×	✓	×	✓	×	✓	×	✓	×	MOO	N/A
[12]	×	✓	×	✓	×	✓	×	×	×	✓	×	VMO	N/A
[4]	×	✓	×	✓	✓	✓	×	✓	✓	✓	×	LP	K-means
[11]	×	×	✓	✓	×	✓	✓	✓	×	✓	×	PSO	N/A
[21]	×	✓	×	✓	×	✓	×	✓	✓	✓	×	MILP	K-medoids
[24]	×	✓	×	✓	×	✓	×	✓	✓	✓	×	GA	N/A
This	✓	✓	✓	✓	✓	✓	✓	✓	✓	✓	✓	PSO-MILP	K-means

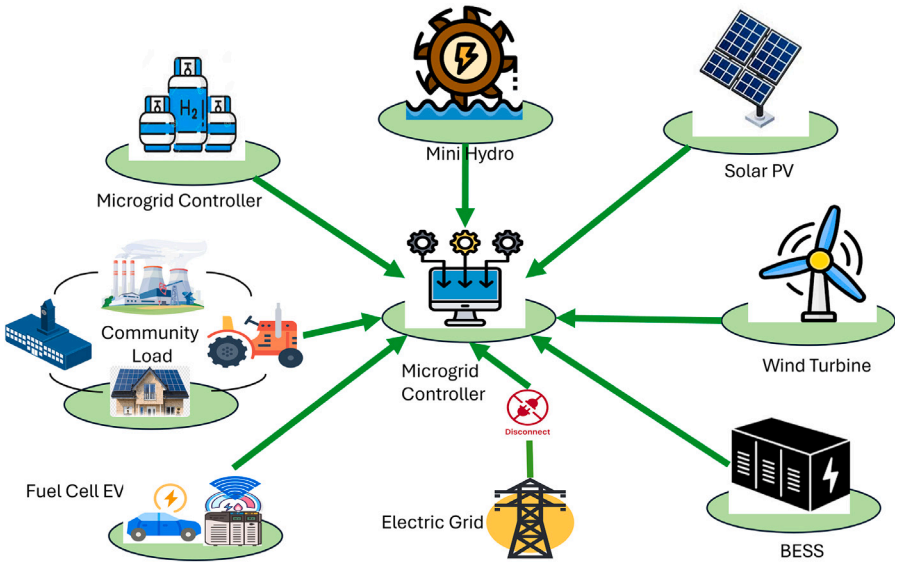

Fig. 1. The schematic diagram of community MG model.

- A novel hybrid algorithm integrating the MLCP approach with a PSO-MILP-based bi-level optimization technique is developed to optimize the capacity and operation of low-voltage future community microgrids.
- Detailed mathematical models are formulated for each RES as well as for energy and emerging FCEV demand to facilitate the clustering algorithm. Moreover, constraints and objective functions for PSO-MILP are developed.
- MLCP algorithm is developed by utilizing K means clustering and data distribution technique to cluster and develop the profile to represent a year long realistic meteorological and energy consumption data.
- Finally, a cost–benefit analysis and carbon emission assessment are conducted on real community MG to evaluate the performance of the proposed system.

The rest of this article is organized in the following manner: Section 2 introduces the system configurations, detailing modeling, cluster analysis, problem formulation, and the optimization process. A case study along with its pertinent data is elaborated upon in Section 3. Section 4 discusses the results and analyses derived from this study. Finally, Section 5 provides a conclusion to this article, summarizing key findings and implications.

2. Methodology

In this section, a thorough explanation of the proposed system's methodology is provided. A detailed representation of the MG's configuration, including its energy sources, storage systems, and community load is presented in Fig. 1. In addition, the process of the transition of the existing system to the MG system is depicted in Fig. 2. In addition, Fig. 3 illustrates the complete workflow of the proposed MLCP-based PSO-MILP system. The flowchart details how PSO is applied to optimize the capacity of RES and storage systems, followed by MILP to manage daily operational costs, ensuring an efficient and cost-effective microgrid operation. The procedure is segmented into three components: 1. Modeling and data processing, 2. Clustering and data preparation, and 3. Optimization and analysis.

2.1. Systems modeling

An energy community is taken into account, where PV, WT, mHydro, BESS, and the hydrogen storage hub (HSH) are presented. In the case of PV and WT, installation constraints are taken into account, while BESS capacity is unrestricted. Furthermore, priority is given to hydrogen demand over BESS charging, and the hydrogen demand must be met from the HSH.

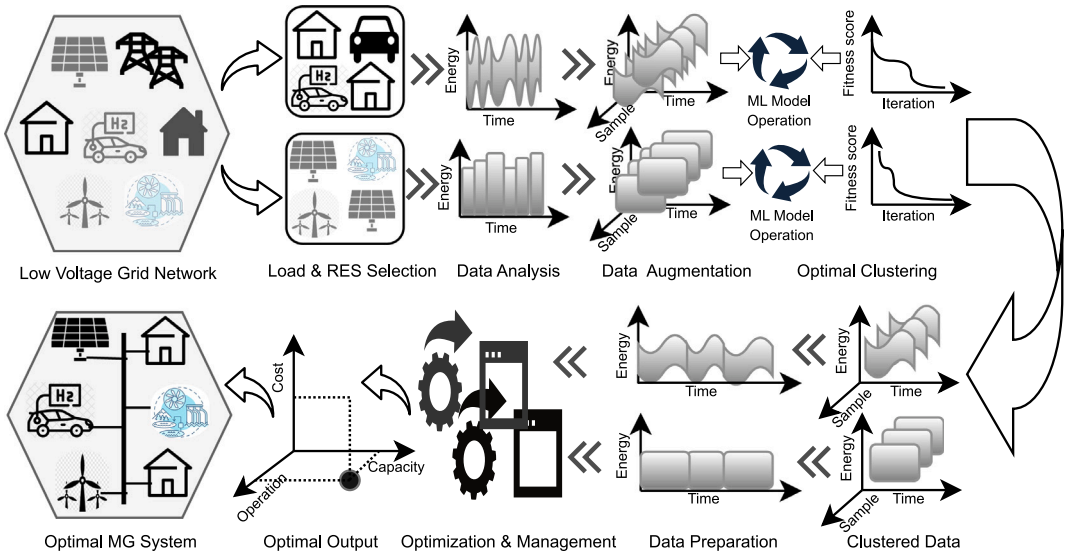

Fig. 2. The schematic diagram of AI based MG transition process.

2.1.1. Network components modeling

The necessary components for the proposed system are elucidated through the mathematical formulation, with real-time data employed to model these components for the analysis.

Grid Power Modeling: As the energy community is interconnected with the grid system, the proposed MG possesses the capacity to both receive and provide energy to the main grid, subject to various operational constraints. The upper and lower limits for importing (im) and exporting (ex) energy to and from the main grid are delineated below:

$$E^{grid}_{im,min} < E^{grid}_{im,t} \leq E^{grid}_{im,max} \tag{1}$$

$$E^{grid}_{ex,min} < E^{grid}_{ex,t} \leq E^{grid}_{ex,max} \tag{2}$$

Photovoltaic Power Modeling: The PV generation power is determined using solar radiation data specific to the designated community location. The power output is determined through a function of solar irradiation ($\mathbb{R}_{PV}$) [31]:

$$E^{PV,M_i}_{G,t} = \begin{cases} E^{PV,M_i}_{G,r}\left(\frac{(\mathbb{R}_{PV,t}\cdot\mathbb{R}_{PV,t})}{\mathbb{R}^{std}_{PV}\cdot\mathbb{R}^{th}_{PV}}\right), \mathbb{R}_{PV,t} \leq \mathbb{R}^{th}_{PV} \\ E^{PV,M_i}_{G,r}\left(\frac{\mathbb{R}_{PV,t}}{\mathbb{R}^{std}_{PV}}\right), \mathbb{R}_{PV,t} > \mathbb{R}^{th}_{PV} \end{cases} \tag{3}$$

$$E^{PV}_{G,t} = \sum_{i=1}^{N_{pv,m}} E^{PV,M_i}_{G,t} \cdot \eta_{PV} \cdot \xi^{M_i}_{PV,t},\ \xi^{M_i}_{PV} \in [1,0] \tag{4}$$

Where, $E^{PV,M_i}_{G,t}$ is the PV power generation of the ith module (M) at time t. where η_{PV} and ξ_{PV} are the overall efficiency and operational status of the PV system, respectively. Assume that the PV power will be generated during the (t_{srt} to t_{end}) period and time step ($s = i \cdot j$) is the function of time interval j. Then the generated energy at each interval and total generated energy within a day (d) can be delineated by Eqs. (5) and (6), respectively.

$$\left[\hat{E}^{PV}_{G,d}\right] = \left(\left[E^{PV}_{G,t}, E^{PV}_{G,t+s_1}, \ldots, E^{PV}_{G,t+t_{end}}\right]\right) \tag{5}$$

$$\forall t \in T_{hr}, \forall T_{hr} \in T, \forall t \in T_{mnt}, \forall T_{mnt} \in T, \forall t \in T_{snd}, \forall T_{snd} \in T$$

$$\hat{E}^{PV,sum}_{G,d} = \sum_{i=0}^{t_{end}} \hat{E}^{PV}_{G,t}(t^{PV}_{srt,t} + s) \tag{6}$$

where $t_{end} \approx n \cdot j$. The following matrix expresses the PV generation for n number of days:

$$\left[\hat{E}^{PV}_{G,d_n}\right] = \begin{bmatrix} E^{PV}_{G,t}, & E^{PV}_{G,t+s_1}, \ldots, & E^{PV}_{G,t+t_{end}} & = \hat{E}^{PV}_{G,d_1} \\ E^{PV}_{G,t}, & E^{PV}_{G,t+s_1}, \ldots, & E^{PV}_{G,t+t_{end}} & = \hat{E}^{PV}_{G,d_2} \\ \vdots & \vdots & \vdots & \vdots \\ E^{PV}_{G,t}, & E^{PV}_{G,t+s_1}, \ldots, & E^{PV}_{G,t+t_{end}} & = \hat{E}^{PV}_{G,d_n} \end{bmatrix} \tag{7}$$

Wind Power Modeling: The WT power output is the function of the several threshold values of wind velocity (w). In this case, cut-in (ci), cut-out (co), and rated (r) values are considered to formulate the equation [11]:

$$E^{W,M_i}_{G,t} = \begin{cases} 0, & w_t < w_{ci} \text{ or } w_{co} > w_t \\ E^{W,M_i}_{G,r}\left(\frac{w_t - w_{ci}}{w_r - w_{ci}}\right)^3, & w_{ci} \leq w_t < w_r \\ E^{W,M_i}_{G,r}, & w_r \leq w_t < w_{co} \end{cases} \tag{8}$$

$$E^{W}_{G,t} = \sum_{i=1}^{N_{w,m}} E^{W,M_i}_{G,t} \cdot \eta_W \cdot \xi^{M_i}_{W},\ \xi^{M_i}_{W} \in [1,0] \tag{9}$$

Where, $E^{W,M_i}_{G,t}$ is the WT power generation of the ith module (M) at time t where η_w and ξ_w are the overall efficiency and operational status of the WT system, respectively. The daily generation at every interval, its cumulative value, and its generation over a specific number of days can be formulated in the following way:

$$\left[\hat{E}^{W}_{G,d}\right] = \left(\left[E^{W}_{G,t}, E^{W}_{G,t+s_1}, \ldots, E^{W}_{G,t+t_{end}}\right]\right) \tag{10}$$

$$\forall t \in T_{hr}, \forall T_{hr} \in T, \forall t \in T_{mnt}, \forall T_{mnt} \in T, \forall t \in T_{snd}, \forall T_{snd} \in T$$

$$\hat{E}^{W,sum}_{G,d} = \sum_{i=0}^{t_{end}} \hat{E}^{W}_{G,t}(t^{W}_{srt,t} + s) \tag{11}$$

$$\left[\hat{E}^{W}_{G,d_n}\right] = \begin{bmatrix} E^{W}_{G,t}, & E^{W}_{G,t+s_1}, \ldots, & E^{W}_{G,t+t_{end}} & = \hat{E}^{W}_{G,d_1} \\ E^{W}_{G,t}, & E^{W}_{G,t+s_1}, \ldots, & E^{W}_{G,t+t_{end}} & = \hat{E}^{W}_{G,d_2} \\ \vdots & \vdots & \vdots & \vdots \\ E^{W}_{G,t}, & E^{W}_{G,t+s_1}, \ldots, & E^{W}_{G,t+t_{end}} & = \hat{E}^{W}_{G,d_n} \end{bmatrix} \tag{12}$$

Mini Hydro Power Modeling: The power produced by mHydro is the function of the water discharge flow rate ($A^{u_i} \cdot v^{u_i}$). The power output from the mHydro unit can be determined as follows:

$$E^{mH,u_i}_{G,t} = \eta^{mH} \cdot \eta^{WD} \cdot \rho \cdot g \cdot hi^{u_i} \cdot A^{u_i} \cdot v^{u_i} \tag{13}$$

$$E^{mH}_{G,t} = \sum_{i=1}^{N_{w,m}} E^{mH,u_i}_{G,t} \cdot \xi^{u_i}_{mH},\ \xi^{u_i}_{mH} \in [1,0] \tag{14}$$

where, $E^{mH,u_i}_{G,t}$ is the power generation of the ith mini hydro unit at time t. where, η^{mH} and η^{WD} are the mHydro and water discharge efficiency, respectively. The operational status of the mHydro unit is defined by binary variable ξ_{mH}.

Microgrid Demand Modeling: The demand profile of a MG is composed of the energy consumption of users in a community. The

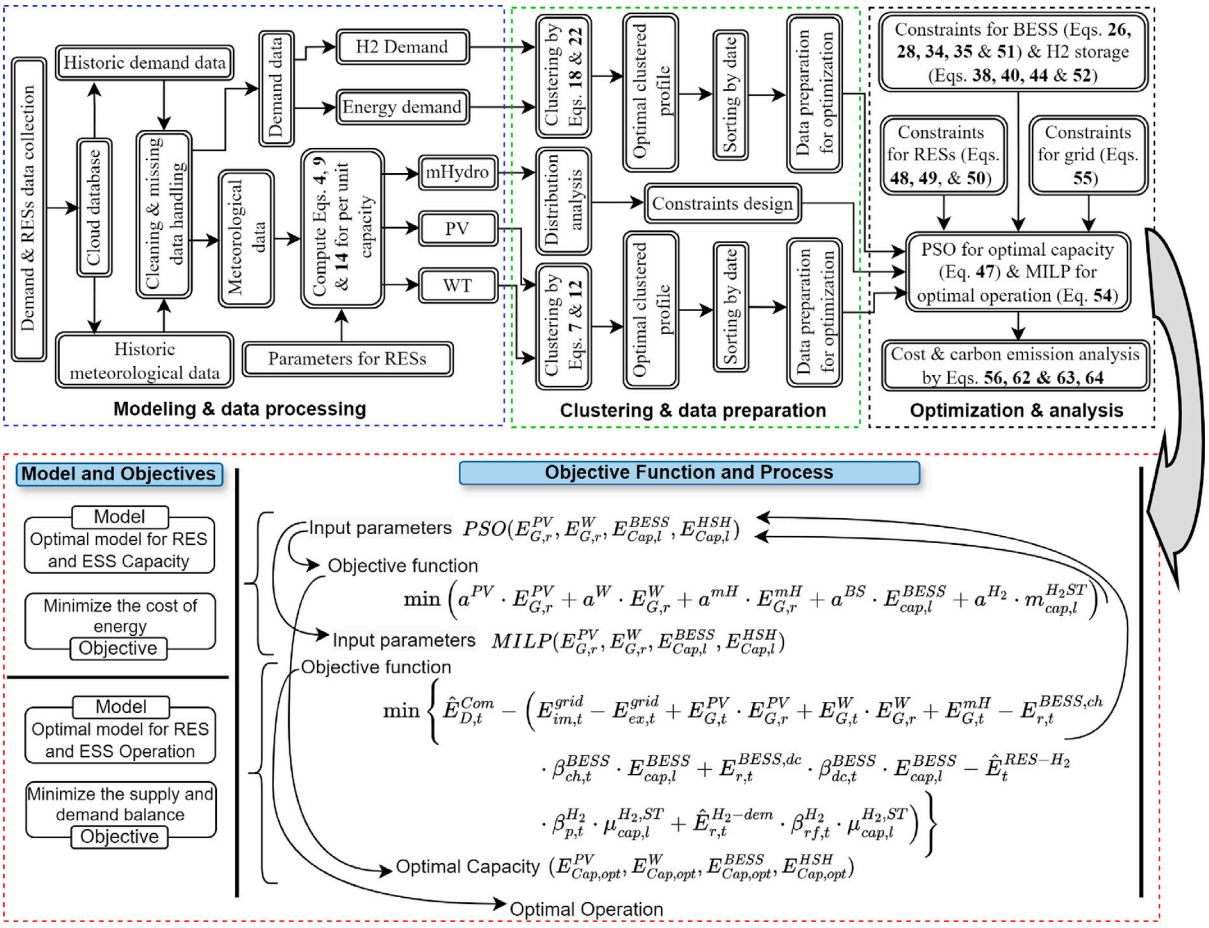

Fig. 3. Workflow for the proposed MLCP-based PSO-MILP system.

energy demand, which is the sum of individual energy consumption, can be presented as follows:

$$\left[\hat{E}^{Com}_{D,t}\right] = \left(\left[\sum_{i=1}^{N_h} E^{H_i}_{D,t}\right]\right), \forall t \in T_{hr}, \forall T_{hr} \in T, \tag{15}$$
$$\forall t \in T_{mnt}, \forall T_{mnt} \in T, \forall t \in T_{snd}, \forall T_{snd} \in T, \forall h \in N_h, \forall H \in \mathbf{H}$$

where, $E^{H_i}_{D,t}$ and $\hat{E}^{Com}_{D,t}$ define the individual user demand and community energy demand at time t, respectively. The daily demand at each interval, its cumulative value, and demand over a particular number of days can be expressed as follows:

$$\left[\hat{E}^{Com}_{D,d}\right] = \left(\left[\hat{E}^{Com}_{D,t}, \hat{E}^{Com}_{D,t+s_1}, \ldots, \hat{E}^{Com}_{D,t+t_{end}}\right]\right) \tag{16}$$
$$\forall t \in T_{hr},\ \forall T_{hr} \in T, \forall t \in T_{mnt},\ \forall T_{mnt} \in T,\ \forall t \in T_{snd}, \forall T_{snd} \in T$$

Then the energy demand of the community at each interval and total energy demand within a day (d) can be delineated by Eqs. (17) and (18), respectively.

$$\hat{E}^{Com,sum}_{D,d} = \sum_{i=0}^{t_{end}} \hat{E}^{Com}_{D,t}(t^{Com}_{srt,t} + s) \tag{17}$$

$$\left[\hat{E}^{Com}_{G,d_n}\right] = \begin{bmatrix} \hat{E}^{Com}_{D,t}, & \hat{E}^{Com}_{D,t+s_1}, \ldots, & \hat{E}^{Com}_{D,t+t_{end}} & = \hat{E}^{Com}_{G,d_1} \\ \hat{E}^{Com}_{D,t}, & \hat{E}^{Com}_{D,t+s_1}, \ldots, & \hat{E}^{Com}_{D,t+t_{end}} & = \hat{E}^{Com}_{G,d_2} \\ \vdots & \vdots & \vdots & \vdots \\ \hat{E}^{Com}_{D,t}, & \hat{E}^{Com}_{D,t+s_1}, \ldots, & \hat{E}^{Com}_{D,t+t_{end}} & = \hat{E}^{Com}_{G,d_n} \end{bmatrix} \tag{18}$$

Fuel Cell Electric Vehicle Demand Modeling: Due to the emergence of fuel cell electric vehicles (FCEV), the demand for these vehicles is taken into consideration by the proposed system. The charging of the FCEV is facilitated by a designated HSH. The hydrogen requirements are the function of the number of FCEV refueling from the HEH at the time t. The following equations can be defined as follows:

$$\left[\hat{H}^{FV}_{D,t}\right] = \left(\left[\sum_{i=1}^{N_v} H^{FV_i}_{D,t}\right]\right), \forall t \in T_{hr}, \forall T_{hr} \in T, \tag{19}$$
$$\forall t \in T_{mnt}, \forall T_{mnt} \in T, \forall t \in T_{snd}, \forall T_{snd} \in T, \forall v \in N_v$$

where, $H^{FV}_{D,t}$ is the hydrogen demand (D) of FCEV at time t. where N_v is the number of FCEV that are refueled from the HSH. Similarly, the Eqs. (20), (21), and (22) represent the hydrogen demand to address the different scenarios:

$$\left[\hat{H}^{FV}_{D,d}\right] = \left(\left[\hat{H}^{FV}_{D,t}, \hat{H}^{FV}_{D,t+s_1}, \ldots, \hat{H}^{FV}_{D,t+t_{end}}\right]\right) \tag{20}$$
$$\forall t \in T_{hr},\ \forall T_{hr} \in T, \forall t \in T_{mnt},\ \forall T_{mnt} \in T,\ \forall t \in T_{snd}, \forall T_{snd} \in T$$

$$\hat{H}^{FV,sum}_{D,d} = \sum_{i=0}^{t_{end}} \hat{H}^{EV}_{D,t}(t^{H_2}_{srt,t} + s) \tag{21}$$

$$\left[\hat{H}^{FV}_{G,D^I}\right] = \begin{bmatrix} \hat{H}^{FV}_{D,t}, & \hat{H}^{FV}_{D,t+s_1}, \ldots, & \hat{H}^{FV}_{D,t+t_{end}} & = \hat{H}^{FV}_{G,d_1} \\ \hat{H}^{FV}_{D,t}, & \hat{H}^{FV}_{D,t+s_1}, \ldots, & \hat{H}^{FV}_{D,t+t_{end}} & = \hat{H}^{FV}_{G,d_2} \\ \vdots & \vdots & \vdots & \vdots \\ \hat{H}^{FV}_{D,t}, & \hat{H}^{FV}_{D,t+s_1}, \ldots, & \hat{H}^{FV}_{D,t+t_{end}} & = \hat{H}^{FV}_{G,d_n} \end{bmatrix} \tag{22}$$

2.1.2. Renewable energy source co-ordination

The energy produced from RES is directed towards the load, BESS, hydrogen generation, and grid. In some situations, excess energy is either stored in the storage system or supplied to the main grid. This mechanism is further articulated through the subsequent mathematical representation.

$$\hat{E}^{RES}_{sur,t} = \hat{E}^{PV}_{sur,t} + \hat{E}^{W}_{sur,t} + \hat{E}^{mH}_{sur,t} \tag{23}$$

$$\hat{E}_{sur,t}^{RES} = \hat{E}_{t}^{RES-BESS} + \hat{E}_{t}^{RES-D} + \hat{E}_{t}^{RES-Grid} + \hat{E}_{t}^{RES-H_2} \quad (24)$$

where $E_{sur,t}^{X}$ denotes the respective surplus amount of energy of the system element X at time t.

2.1.3. Storage model component

To enhance the reliability of energy quality, storage systems are incorporated into the system. Given the higher uncertainty associated with RES, storage systems play a crucial role in ensuring a continuous energy supply. Within the framework of the proposed system, two storage systems such as BESS and HSH are included. Details regarding the configuration of these storage systems are provided in the subsequent subsection.

Battery Energy Storage System Setting: The function of BESS is to supply energy to the MG in the absence of sufficient energy to mitigate the demand. The required parameters and constraints related to the BESS are considered to model the BESS. The following equation depicts the configuration of BESS within a MG.

$$\hat{E}_{ch,t}^{BESS} = \hat{E}_{t}^{RES-BESS} \times \eta_{eff,ch}^{BESS} \quad (25)$$

$$\hat{E}_{r,min}^{BESS,ch} < \hat{E}_{r,t}^{BESS,ch} \leq \hat{E}_{r,max}^{BESS,ch} \quad (26)$$

$$\hat{E}_{dc,t}^{BESS} = \hat{E}_{t}^{BESS} \times \eta_{eff,dc}^{BESS} \quad (27)$$

$$\hat{E}_{r,min}^{BESS,dc} < \hat{E}_{r,t}^{BESS,dc} \leq \hat{E}_{r,max}^{BESS,dc} \quad (28)$$

$$\hat{E}_{ch,t}^{BESS} \approx \hat{E}_{r,t}^{BESS,ch} \quad (29)$$

$$\hat{E}_{r,t}^{BESS,dc} \approx \hat{E}_{t}^{BESS-D} \quad (30)$$

where $\hat{E}_{ch,t}^{BESS}$ and $\hat{E}_{dc,t}^{BESS}$ are the charging and discharging energy at time t, respectively. The state of charge (SOC) is the function of the initial SOC and the charging and discharging energy of the BESS. It can be defined as follows:

$$S\hat{O}C_{t}^{BESS} = S\hat{O}C_{t-1}^{BESS} + \left(\frac{\hat{E}_{r,t}^{BESS,ch} \cdot \beta_{ch}^{BESS} - \hat{E}_{r,t}^{BESS,dc} \cdot \beta_{dc}^{BESS}}{\hat{E}_{Cap}^{BESS}} \right) \quad (31)$$

$$\beta_{ch}^{BESS} + \beta_{dc}^{BESS} = 1,\ \beta^{BESS} \in [1,0] \quad (32)$$

$$S\hat{O}C_{t-1}^{BESS} \approx S\hat{O}C_{ini}^{BESS}, \text{where} \quad t = 1 \quad (33)$$

$$S\hat{O}C_{min}^{BESS} < S\hat{O}C_{t}^{BESS} \leq S\hat{O}C_{max}^{BESS} \quad (34)$$

$$E_{G,t}^{PV} \leq \hat{E}_{D,t}^{Com} \quad (35)$$

where β_{ch}^{BESS} and β_{dc}^{BESS} are the charging discharging indicator binary variables.

Hydrogen Storage Setting The aim of integrating the HSH is to generate and store hydrogen in the storage system for supplying the FCEV. The hydrogen will be produced from the excess PV and WT generation. The liquid hydrogen will be stored in the HSH tank to mitigate the FCEV demand. The quantity of renewable energy necessary to drive the water electrolyzer within a standard H_2 refueling station for the production of hydrogen (measured in kilograms) can be derived as follows:

$$m_{p,t}^{RES-H_2} = \frac{\eta_{els}^{H_2} \times \hat{E}_{t}^{RES-H_2}}{EI^{els}} \quad (36)$$

$$m_{r,t}^{H_2,p} \approx m_{p,t}^{RES-H_2} \quad (37)$$

$$m_{r,min}^{H_2,p} < m_{r,t}^{H_2,p} \leq m_{r,max}^{H_2,p} \quad (38)$$

$$m_{r,t}^{H_2-FV} = m_{r,t}^{H_2,rf} \quad (39)$$

$$m_{r,min}^{H_2,rf} < m_{r,t}^{H_2,rf} \leq m_{r,max}^{H_2,rf} \quad (40)$$

$$m_{t-1}^{H_2,ST} \approx m_{ini}^{H_2,ST}, \quad \text{where} \quad t = 1 \quad (41)$$

$$m_{t}^{H_2,ST} = m_{t-1}^{H_2,ST} + m_{p,t}^{RES-H_2} \cdot \beta_{p}^{H_2} - m_{rf,t}^{H_2-FV} \cdot \beta_{rf}^{H_2},\ \beta^{H_2} \in [1,0] \quad (42)$$

where $m_{H_2-Prod_h}$ represents the mass of hydrogen produced. EI^{els} signifies the energy intensity of the optimal water electrolyzer's output, specifically hydrogen. The value of EI^{els} is set at 0.039 MWh/kg-H_2 [32]. The symbol $\eta_{els}^{H_2}$ is indicative of the electrolyzer's efficiency. The amount of hydrogen in the HSH tank can be denoted as the state of hydrogen (SOH). Therefore, the SOH can be defined as follows:

$$SOH_{t}^{H_2} = \frac{m_{t}^{H_2,ST}}{m_{Cap}^{H_2,ST}} \quad (43)$$

$$SOH_{min}^{H_2} < SOH_{t}^{H_2} \leq SOH_{max}^{H_2} \quad (44)$$

2.1.4. Tariff setting

In the proposed system, real tariff data collected from the energy community are utilized. The grid flat tariff (GFT) is calculated taking into account the daily allowance for energy consumption of the community. In addition, the time-of-use (ToU) pricing is also considered to calculate the daily energy cost. Those equations are formulated as follows:

$$TF_{t}^{f} = \begin{cases} TF_{t}^{f_1}, & \text{if} \quad 0 < E_{D}^{Com} < E_{D}^{Com,f_1} \\ TF_{t}^{f_2}, & \text{if} \quad E_{D}^{Com,f_1} \leq E_{D}^{Com} < E_{D}^{Com,f_2} \\ TF_{t}^{f_n}, & \text{if} \quad E_{D}^{Com,f_2} \leq E_{D}^{Com} \leq E_{D}^{Com,f_n} \end{cases} \quad (45)$$

$$TF_{t}^{ToU} = \begin{cases} TF_{t}^{op}, & \text{if} \quad t_{op}^{srt} \leq t < t_{op}^{end} \\ TF_{t}^{mp}, & \text{if} \quad t_{mp}^{srt} \leq t < t_{mp}^{end} \\ TF_{t}^{pk}, & \text{if} \quad t_{pk}^{srt} \leq t \leq t_{pk}^{end} \end{cases} \quad (46)$$

where T_{t}^{op}, T_{t}^{mp}, and T_{t}^{pk} are the tariff amounts in the off-peak, medium-peak, and peak periods.

2.2. Data clustering and profiling

In the study, non-dispatchable RES and demand are clustered to ascertain the optimal daily demand and generation profile, aiming to achieve the best capacity of RES under various configurations. In this study, we utilize the MLCP strategy, with the procedures comprehensively outlined in Algorithm 1 (see Fig. 4). The algorithm is divided into two key sections: the initial part focuses on clustering, while the latter is dedicated to approaches for data profiling. For the clustering phase, the K-means clustering technique is employed. Eqs. (7), (12), (18), and (22) serve as inputs for the K-means algorithm, facilitating the clustering of daily generation and consumption profiles. Initially, the selection of the optimal cluster number is made by analyzing one-year historical data concerning demand and RES generation. Following this, the optimal number of clusters is established. Subsequently, utilizing this optimal cluster number, a profile is constructed. For demand, the maximum value from each cluster is selected. Conversely, for generation, the minimum value from each cluster is chosen. Finally, the profiles are organized by date to ensure consistency between the generation and demand profiles.

2.3. Optimal capacity and operation

The determination of the optimal capacity and operational strategies for RESs and storage systems is achieved using the PSO-MILP algorithm. This PSO algorithm is particularly applied in the context of ascertaining optimal capacities. For the formulation of this optimization

Algorithm 1 Data clustering and profiling algorithm

Input: (Historical data)
Collection & cleaning
Duplicate & missing data handling
Re-sampling & normalization
Preparation ($X \leftarrow$ data (Eqs. 7, 12, 18, & 22))
Function **ElbowMethod**(X, n)
for i in n **do**
  $kmeans \leftarrow KMeans(n_c = i)$
  $kmeans.fit\_predict(X)$
  $ds \leftarrow kmeans.inertia$
end for
plotElbowGraph(ds)
$o_c \leftarrow$ **findElbowPoint**(ds)
return o_c
$kmeans$ with $n\_c = o_c$
$c \leftarrow kmeans.fit\_predict(X)$
$c_{sr} \leftarrow$ pd.Series($c, name = ' cluster'$)
$C_d \leftarrow data$.set_index(c_{sr}, append=True)
Distribution in a cluster
for i in o_c **do**
  $T \leftarrow C_d$ of i_{th} cluster
  $C_p \leftarrow$ max/min/mean profile of T
end for
Sorting by date (C_p)
Generate profile
end

(a)

Algorithm 2 Optimal capacity and operation algorithm

Define constants $\hat{E}^{BESS,ch}_{r,t}, \hat{E}^{BESS,dc}_{r,t}, m^{H_2,rf}_{r,t}, o_c \cdot s.$
Read data from **Algorithm 1** and TF^f_t, TF^{ToU}_t.
function OPTIMIZE_CAPACITY
  Define MILP model
  Define decision variables $\beta^{BESS}_{ch,t}, \beta^{BESS}_{dc,t}, \beta^{H2}_{p,t}, \beta^{H2}_{rf,t}$
  Define $S\hat{O}C^{BESS}_{ini}, m^{H_2,ST}_{ini}$
  Define an objective function by Eq. (47)
  for each time period t **do**
    Constraints for BESS by Eq. (26), (28), (34), (35)
    Constraints for H2 by Eq. (38), (40), (44)
    Energy balance constraint by Eq. (54), (55),
    binary constraints by Eq. (32)
  end for
  Optimize the model
end function
Define constraints by Eqs. (48), (49), (50), (51), (52)
PSO algorithm to optimize capacities:
Set initial capacities within bounds
Optimize capacities
Find the optimal PV, BESS, and Hydro capacities

(b)

Fig. 4. (a) Algorithm 1 and (b) Algorithm 2.

problem, the objective function alongside the constraints applicable to each RES is articulated in the following manner:

$$min \left| \alpha^{PV} \cdot E^{PV}_{G,r} + \alpha^{W} \cdot E^{W}_{G,r} + \alpha^{mH} \cdot E^{mH}_{G,r} + \alpha^{BS} \cdot E^{BESS}_{Cap,l} + \alpha^{H_2} \cdot m^{H_2,ST}_{Cap,l} \right| \tag{47}$$

$$E^{PV}_{Cap,min} < E^{PV}_{G,r} \leq E^{PV}_{Cap,max} \tag{48}$$

$$E^{W}_{Cap,min} < E^{W}_{G,r} \leq E^{W}_{Cap,max} \tag{49}$$

$$E^{mH}_{Cap,min} < E^{mH}_{G,t} \leq E^{mH}_{Cap,max} \tag{50}$$

$$\hat{E}^{BESS}_{Cap,min} < \hat{E}^{BESS}_{Cap,l} \leq \hat{E}^{BESS}_{Cap,max} \tag{51}$$

$$m^{H_2,ST}_{Cap,min} < m^{H_2,ST}_{Cap,l} \leq m^{H_2,ST}_{Cap,max} \tag{52}$$

$$\alpha = \frac{\mathbb{C}_{cc} \cdot o_c}{\mathbb{Y} \cdot d} \tag{53}$$

By using capital cost ($\mathbb{C}_{cc}$), the optimal number of cluster (o_c), and the lifetime ($\mathbb{Y}$) of the RESs, the optimization factor (α) is calculated by Eq. (54).

The MILP optimization algorithm is applied to find the optimal scheduling of RES and storage systems. However, it is assumed that the energy supplied by the grid originates from carbon-based power generation plants. Furthermore, the MG is restricted from supplying energy back to the grid. This scenario can be referred to as an "islanded operational mode", signifying that no energy transactions will take place between the utility grid and the MG. Consequently, the objective function will be designed in such a way that the grid export and import energy should be zero and can be expressed by Eq. (54). The integrated PSO-MILP is depicted in Algorithm 2 (see Fig. 4).

$$\begin{aligned} min \Big| \hat{E}^{Com}_{D,t} - (E^{grid}_{im,t} - E^{grid}_{ex,t} + E^{PV}_{G,t} + E^{W}_{G,t} + E^{mH}_{G,t} \\ - E^{BESS,ch}_{r,t} \cdot \beta^{BESS}_{ch,t} + E^{BESS,dc}_{r,t} \cdot \beta^{BESS}_{dc,t} \\ - \hat{E}^{RES-H_2}_{t} \cdot \beta^{H_2}_{p,t} + \hat{E}^{H_2-dem}_{r,t} \cdot \beta^{H_2}_{rf,t}) \Big| \end{aligned} \tag{54}$$

$$E^{grid}_{im,t} \approx 0 \text{ and } E^{grid}_{ex,t} \approx 0 \tag{55}$$

2.4. Cost analysis

The cost of energy (COE) is determined by the net present cost (NPC) and capital recovery factors (CRFs) of system components and electricity, in addition to the yearly electricity demand. The following equations represent the cost analysis of the proposed system [11].

$$COE_{mg} = \frac{NPC_{mg} \cdot CRF_{mg}}{\sum_{c=1}^{o_c} \hat{E}^{Com,sum}_{D,d,c} + \hat{H}^{FV,sum}_{D,d,c}} \tag{56}$$

$$CRF_{mg} = \frac{\sigma \cdot (1+\sigma)^n}{(1+\sigma)^{n-1}} \tag{57}$$

$$\begin{aligned} NPC_{mg} = E^{PV}_{Cap,opt} \cdot \mathbb{C}^{PV}_{fact} + E^{W}_{Cap,opt} \cdot \mathbb{C}^{W}_{fact} + E^{BESS}_{Cap,opt} \cdot \mathbb{C}^{BESS}_{fact} \\ + E^{mH}_{Cap,opt} \cdot \mathbb{C}^{mH}_{fact} + E^{H_2}_{Cap,opt} \cdot \mathbb{C}^{H_2}_{fact} \end{aligned} \tag{58}$$

$$\mathbb{C}_{fact} = (\mathbb{C}_{cc} + \mathbb{C}_{mc} + \mathbb{C}_{rc}) \tag{59}$$

$$\mathbb{C}_{mc} = \frac{\mathbb{C}_{mc} \cdot (1+\gamma)^{\mathbb{Y}-1}}{\gamma \cdot (1+\gamma)^{\mathbb{Y}}} \tag{60}$$

$$\mathbb{C}_{rc} = \mathbb{C}_{rc} \cdot \sum_{t=1}^{t<y<\mathbb{Y}} \frac{1}{(1+\gamma)^{ty}} \tag{61}$$

where, γ and σ denote the interest rate and discount rate, respectively. Additionally, $\mathbb{C}_{fact}$, $\mathbb{C}_{cc}$, $\mathbb{C}_{mc}$, and $\mathbb{C}_{rc}$ represent the aggregated cost factor, capital cost, maintenance cost factor, and replacement cost factor, respectively. By considering the existing tariff, the energy cost of the community ($\mathbb{C}^{Com}_{G}$) can be determined by Eq. (62). The tariff data is collected from the local community.

$$\mathbb{C}^{Com}_{G} = \sum_{c=1}^{o_c} \sum_{t=1}^{T} \left(\hat{E}^{Com}_{D,t,c} + \hat{H}^{FV}_{D,t,c} \right) \cdot TF^{ToU}_t \text{ or } TF^{f}_t \tag{62}$$

The equivalent carbon emissions (CE) from the energy community before and after the transition of the MG are defined in Eqs. (63) and (64). Different values of carbon emissions factor (CEF) for the different technologies are considered [33].

$$CE_{non-RES} = \sum_{c=1}^{o_c} \left(\hat{E}^{H_h,sum}_{D,d,c} + \hat{H}^{FV,sum}_{D,d,c} \right) \cdot CEF \tag{63}$$

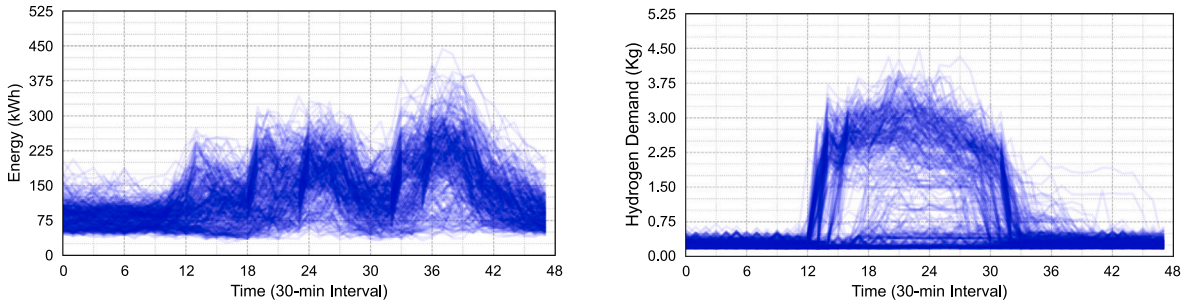

(a) (b)

Fig. 5. Historical data of (a) Electricity demand, (b) H_2 demand.

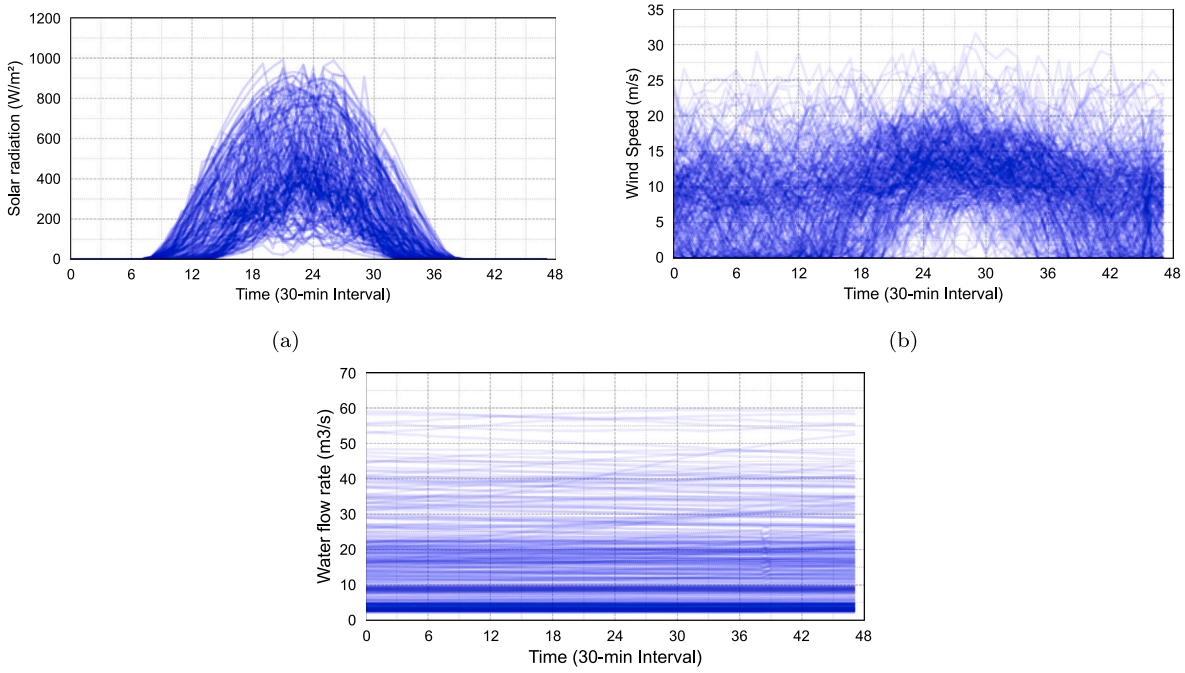

(a) (b) (c)

Fig. 6. Historical data of (a) Solar irradiation, (b) Wind speed, (c) Water flow.

$$CE_{RES} = \left(E^{PV}_{Cap,opt} + E^{W}_{Cap,opt} + E^{mH}_{Cap,opt} + E^{BESS}_{Cap,opt}\right) \cdot CEF \quad (64)$$

3. Case study overview

The demand and RES generation-related data are taken from a region of Tasmania, Australia. Real energy demand and RES parameters data from the community are utilized, spanning one year. This data is segmented into 30-minute intervals, resulting in 48 data samples per day. Different data cleaning and processing approaches are applied to clean the data, including anomaly removal and missing data filling. Addressing a real-time issue, the actual tariff plan provided by the local energy supplier is considered. Python programming is employed to develop and implement the proposed model and a hybrid optimization algorithm. The MILP for optimal power flow is solved using the Gurobi optimizer (version 10.0.3), while the PSO method is applied to determine the optimal capacity. The hardware used for this process includes a high-performance computer equipped with 64 GB of RAM and an Intel® Xeon® E-2288G CPU, operating at 3.70 GHz.

The subsequent sections will delve into the diverse input data needed for the proposed scheme, encompassing both technical and financial parameters.

3.1. Energy and hydrogen demand

Fig. 5(a) displays the actual daily energy demand, measured at half-hourly intervals, over one year, resulting in 48 data samples per day. This figure provides a comprehensive visual representation of the MG's energy demand. Similarly, Fig. 5(b) portrays the hydrogen demand for FCEV, expressing the demand in kilograms. In the absence of hydrogen demand data at 30-minute intervals for the MG area, synthetic data was produced through an analysis based on fuel demand.

3.2. RES parameters and constraints

Upon investigating the availability and limitations of RESs within the energy community, systems such as PV, WT, and mHydro have been chosen for the proposed setup. The primary determinants for the generation of these RESs include solar irradiation, wind speed, and water flow rate. Figs. 6(a), 6(b), and 6(c) present historical data on solar radiation, wind speed, and water discharge flow rate, respectively, within the energy community. In addition, the required parameters of PV, WT, and mini-hydro are presented in Tables 2, 3, and 4, respectively.

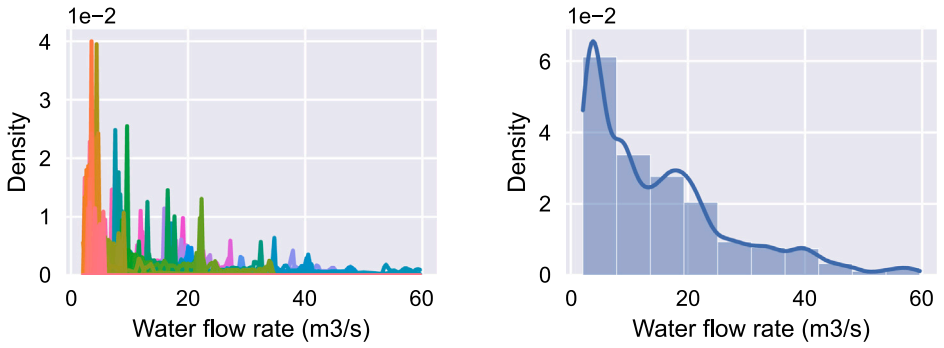

(a) (b)

Fig. 7. Data distribution of water flow rate (a) and (b).

Table 2
The required parameters of PV system.

Parametres		Parametres	
$\mathbb{R}_{PV}^{std}$	1000 W/m2	η_{PV}	95%
$\mathbb{R}_{PV}^{th}$	50 W/m2	$E_{max}^{PV,Cap}$	350 kW

Table 3
The required parameters of WT system.

Parameters		Parameters	
w_{co}	25 m/s	w_{ci}	3.5 m/s
w_r	13 m/s	η_W	85%
$E_{min}^{W,Cap}$	200 kW	$E_{max}^{W,Cap}$	350 kW

Table 4
The required parameters of mHydro.

Parameters		Water flow rate (m3/s)	
h^{u_i}	5 m	min	2.07
ρ	1000 kg/m^3	max	59.58
g	9.81 m/s^2	mean	15.06
η^{TE}	40%	50% of data	11.76
η^{WD}	45%	75% of data	20.73

However, while both PV and WT are non-dispatchable RES, mHydro can be dispatchable. The minimum and maximum energy supply capacities of the mHydro are calculated based on the distribution of water flow rates. Table 4 illustrates various parameters along with the percentage distribution of data. Following this analysis, the maximum and minimum energy supply capacities for the mHydro have been established at 25 kWh and 100 kWh, respectively.

3.3. Storage parameters and constraints

In this study, the BESS is characterized by essential parameters like capacity, power rating, SOC, and round-trip efficiency. Additionally, constraints such as charge and discharge rates, and minimum and maximum SOC are also considered. Table 5 displays the BESS's properties utilized in the experiment. Similarly, the HSH features comparable parameters and constraints, which include EI, maximum production and supply volumes, and the efficiency of converting electrical energy into hydrogen. The HSH's maximum tank capacity and the minimum quantity to be maintained in the tank are also taken into account. The properties of this HSH are outlined in Table 6.

3.4. Microgrid cost and grid tariff

As the proposed system accounts for transitioning the current energy system into an MG, the assumption is that the system already possesses an established energy distribution network, encompassing distribution lines, transformers, and other electrical equipment. Accordingly, the focus has been on considering the capital, operational, and maintenance (O&M) costs of the RES rather than the installation costs of the network. Table 7 presents the costs of RES and storage system [34,35]. In addition, three distinct tariff types are evaluated based on the energy rates provided by suppliers within the energy community. These tariffs include the low voltage residential general (FT-1), low voltage business general (FT-2), and low voltage business time of use tariff (ToU). A half-hourly tariff interval profile throughout the day is depicted in Fig. 8.

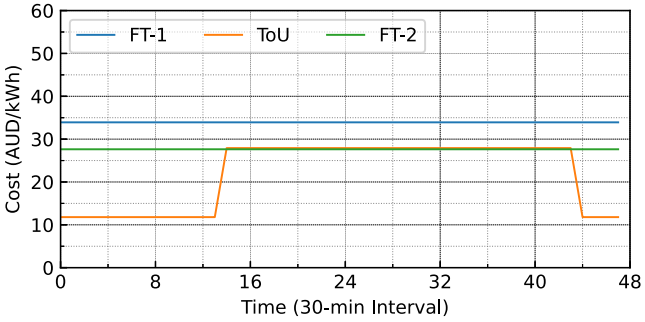

Fig. 8. Different types of tariff used in the case study.

Table 5
The required parameters of BESS.

Parameters		Constraints	
$\eta_{eff,c}^{BS}$	95%	$\hat{SoC}_{min}^{BS}$	20%
$\eta_{eff,dc}^{BS}$	95%	$\hat{SoC}_{max}^{BS}$	100%
$\hat{E}_{r,max}^{BS,c}$	200 kWh/interval	$E_{max}^{BS,Cap}$	3000
$\hat{E}_{r,max}^{BS,dc}$	250 kWh/interval	$E_{min}^{BS,Cap}$	0

Table 6
The required parameters of H2 storage.

Parametres		Parametres	
$\eta_{els}^{H_2}$	95%	$m_{SoH,min}^{H_2,ST}$	20%
$LEIE_{ls}$	0.039 MWh/kg-H2	$m_{SoH,max}^{H_2,ST}$	100%
$m_{r,max}^{H_2,g}$	10 Kg/FCEHV	$M_{max}^{H_2,Cap}$	70 kg
$\hat{E}_{r,max}^{H_2-dem}$	5 Kg/FCEHV	$M_{min}^{H_2,Cap}$	0 kg

4. Simulation result

The demand and RES generation-related data are taken from a region of Tasmania, Australia. Real energy demand and RES parameters

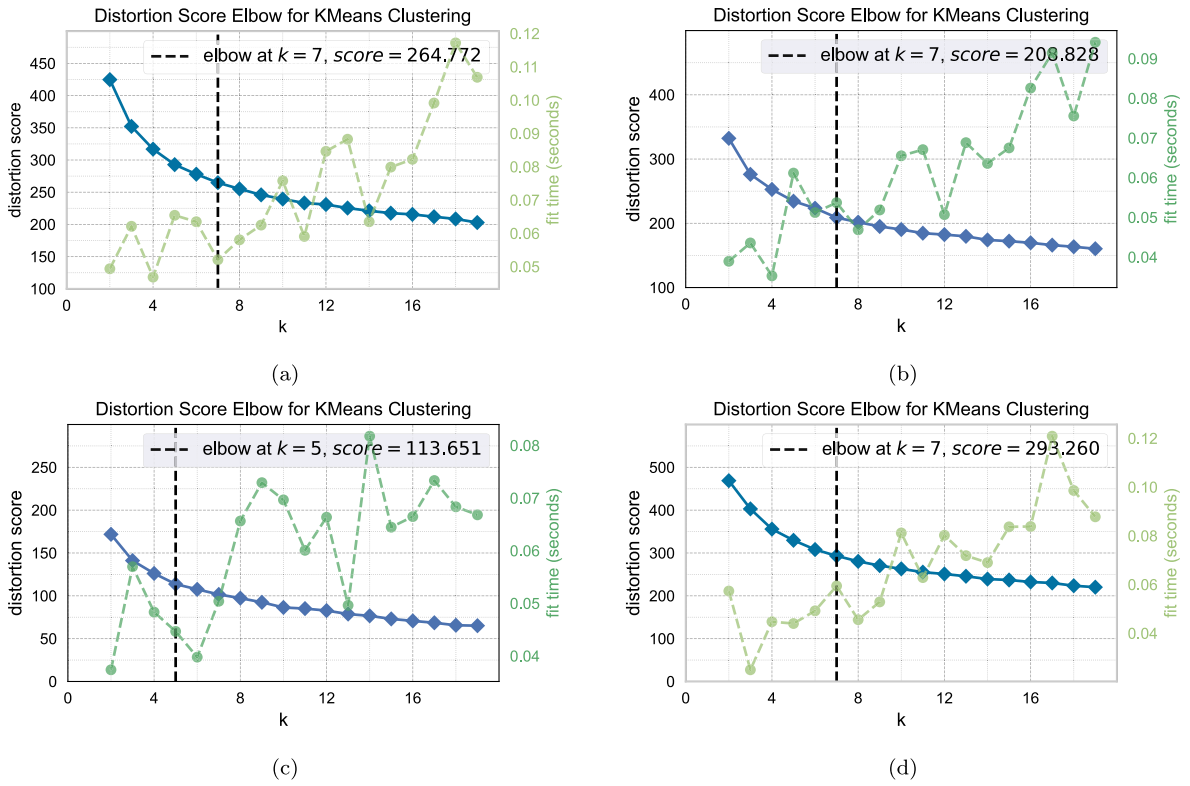

Fig. 9. Optimal cluster results (a) Electricity demand, (b) H_2 demand, (c) PV generation, and (d) WT generation.

Table 7
The cost of RES and storage system in AUD/kW.

RES name	Capital Cost/kW	O&M Cost/kW	Rep Cost/kW	Year
PV	1441	17	300	10
WT	1950	25	300	10
BESS	2296	300	300	10
Hydrogen	8032	1000	600	10
mHydro	2185	48.07	300	10

Table 8
Optimal capacity of RESs and storage system.

PV(kW)	WT (kW)	BESS (kWh)	Hydrogen (Kg)	mHydro (min -max)(kW)
280.27	240	2490	48.47	25-100

data from the community are utilized, spanning one year. This data is segmented into 30-minute intervals, resulting in 48 data samples per day. Different data cleaning and processing approaches are applied to clean the data, including anomaly removal and missing data filling. To address a real-time issue, the actual tariff plan provided by the local energy supplier is considered. Python programming is employed to develop and implement the proposed model and a hybrid optimization algorithm. The MILP for optimal power flow is solved using the Gurobi optimizer (version 10.0.3), while the PSO method is applied to determine the optimal capacity. The hardware used for this process includes a high-performance computer equipped with 64 GB of RAM and an Intel® Xeon® E-2288G CPU, operating at 3.70 GHz. The simulation results obtained from the proposed system are described in the following:

4.1. Optimal cluster and data preparation for optimization

Algorithm 1 (see Fig. 4) is employed to prepare data for both energy demand and hydrogen demand. The resulting optimal number of clusters for both energy and hydrogen demand within the energy community is depicted in Figs. 9(a) and 9(b). These figures reveal that the optimal cluster number for both scenarios is 7. Additionally, the clustered data for both energy demand and hydrogen demand are displayed in Figs. 10(a) and 10(b).

Due to the dispatchable nature of mini-hydro generation, a different approach is taken: instead of clustering analysis, the minimum and maximum energy supply amounts are selected, with data distribution analysis presented in Fig. 7. Conversely, for both PV and WT generation, Algorithm 1 (see Fig. 4) is used to prepare the data. For PV, the optimal number of clusters identified is 5, as shown in Fig. 9(c). Given that most profiles are clustered into 7 groups, an additional 2 clusters are chosen based on data distribution, and their average values are utilized to form a 7-cluster structure. In the case of WT, the optimal number of clusters is found to be 7, which is detailed in Fig. 9(d). Consequently, the clustered data for both energy demand and hydrogen demand are illustrated in Figs. 10(c) and 10(d).

4.2. Optimal capacity of renewable energy sources and storage

The optimal capacity for the RES and storage system aims to secure a reliable and effective energy setup for the community. The higher uncertainties associated with RES, increasing the storage system's capacity will lower the chances of energy disruptions. The optimization process is conducted on the total clustered data, which effectively addresses the uncertainty issues related to demand and generation. The MLCP algorithm is applied for proper clustering and profiling the data. Fig. 10 presents the optimal number of clusters of the data of each component. It can be observed that the optimal cluster of the most components is 7. Consequently, 30-minute intervals of 7 days of data are chosen for the optimization process.

However, the size should be chosen to minimize the costs. Consequently, capacities are determined by the optimization algorithm

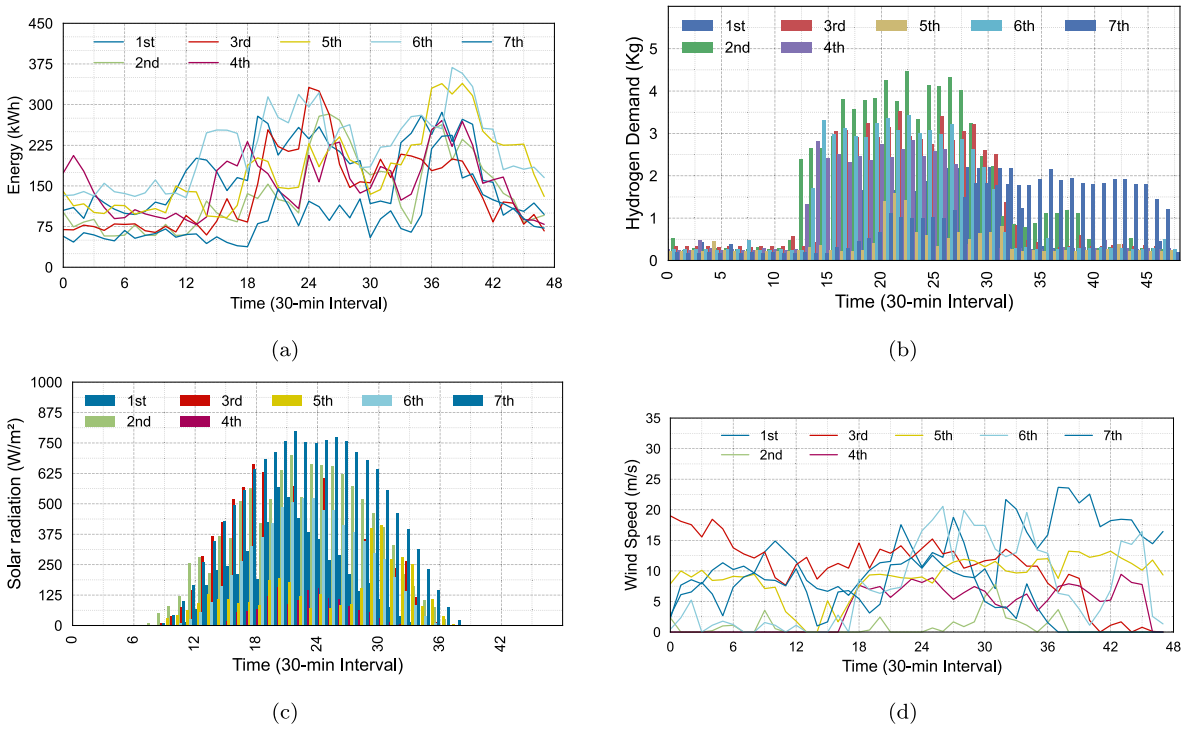

Fig. 10. Optimal clustered profile of (a) Electricity demand, (b) H_2 demand, (c) PV generation, and (d) WT generation.

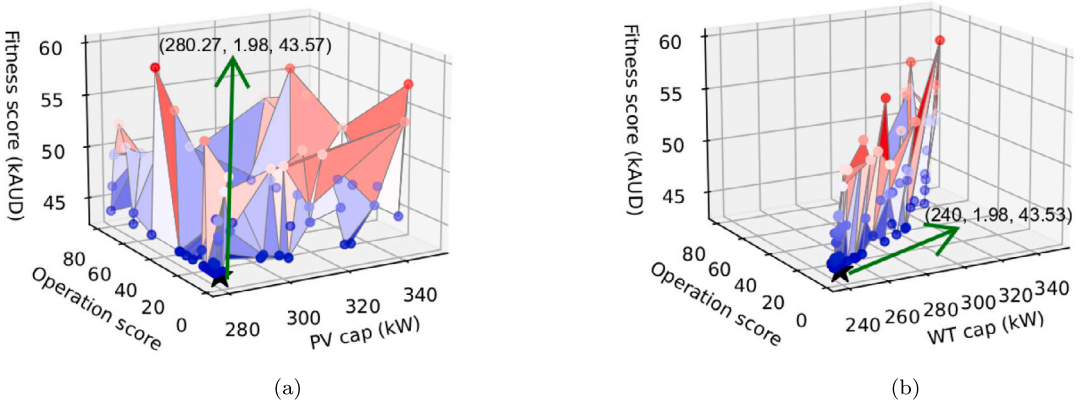

Fig. 11. Optimization results (a) PV capacity and (b) WT capacity in kW.

based on the actual values of the α. The α values for various RESs and storage systems are derived from their capital costs, with the values being 2.76 for PV, 3.74 for WT, 4.40 for BESS, 15.40 for HSH, and 4.19 for mHydro. Table 8 displays the optimal capacities of RESs and storage systems for the proposed MG system. The PV system, having the lowest value of the α, aids the objective function in achieving a higher capacity for PV. This principle is similarly applicable to WT, mHydro, and BESS systems. Their respective α values influence the objective function to favor optimal capacities. For HSH, concrete constraints are employed to ensure that the value of the α does not significantly impact the determination of the optimal capacity. Additionally, the convergence graph for PV, WT, BESS, and HSH are presented in Figs. 11 and 12, respectively. However, the increased BESS capacity aims to enhance system reliability. Consequently, the MG can ensure adequate energy supply to the community even during periods of very low RES generation.

4.3. Optimal energy flow of the microgrid

The optimal energy flow within the MG dictates how the MG operates efficiently and seamlessly. Analyzing the various scenarios involving RES generation and MG energy demand ensures the MG's sustainability and reliability. Figs. 13(a) and 13(b) depict the overall energy supply and demand of the MG across seven consecutive clusters. The figure reveals various demand patterns that validate the system's performance, including sensitivity analysis. Table 9 provides comprehensive data on total energy demand, supply, and generation levels, as well as the discrepancies between supply and demand, and generation and demand.

Several key insights can be gleaned from these differences. Negative values in the demand-generation difference indicate that surplus energy is stored in the storage system, as indicated by the arrow symbol. Conversely, positive values in the demand-generation difference signify

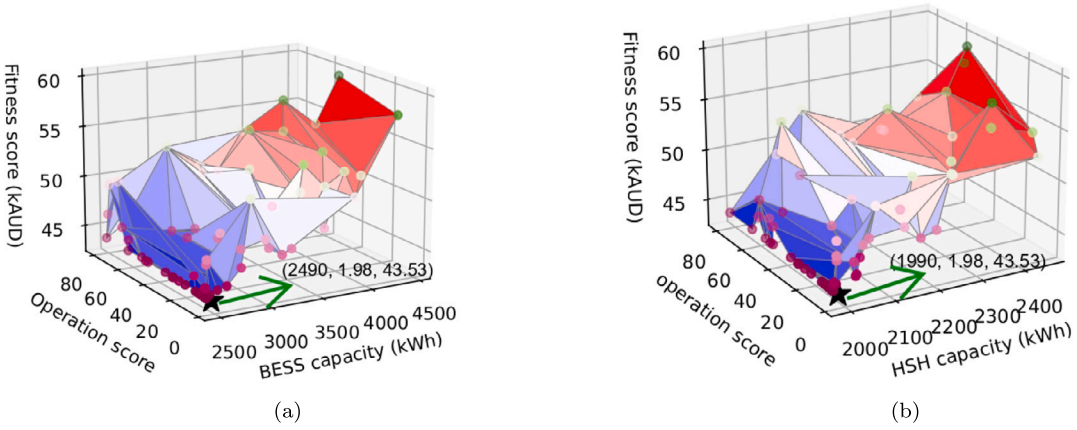

Fig. 12. Optimization results (a) BESS capacity and (b) HSH capacity in kWh.

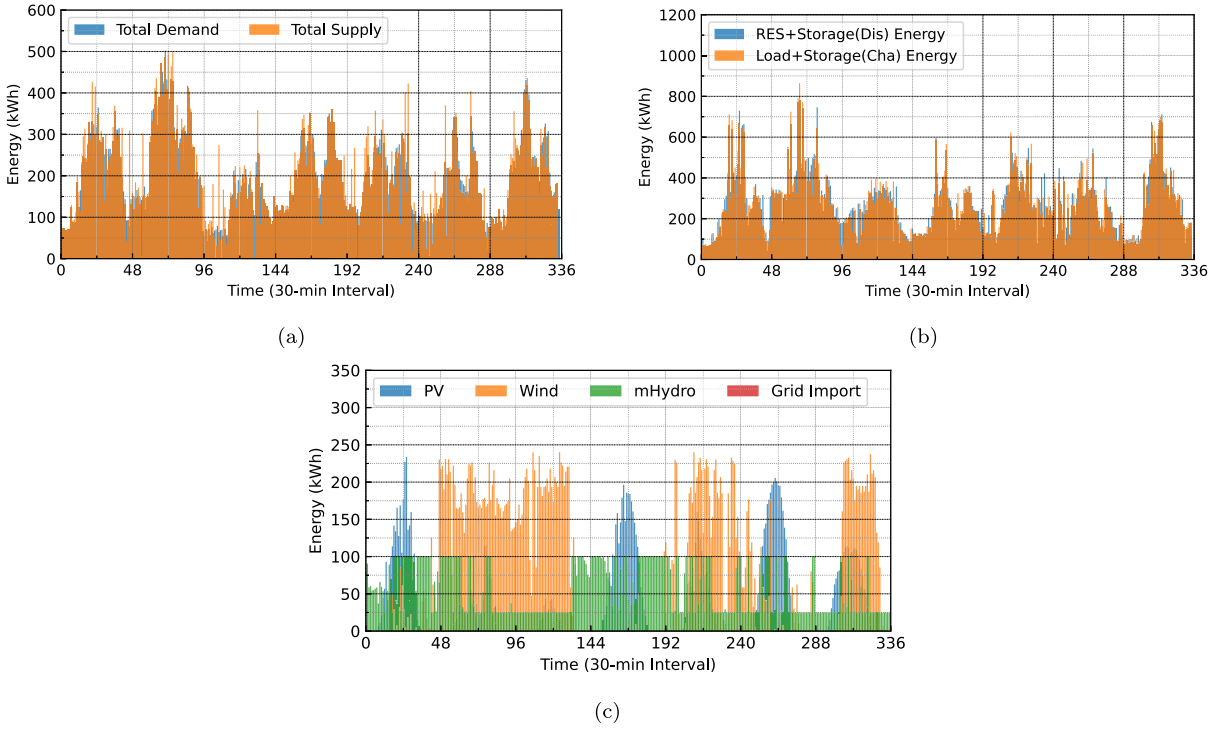

Fig. 13. Optimization result (a) demand and supply profile, (b) RES generation, charge and discharge, and demand, and (c) RES energy supply during the operation period.

Table 9
Optimal energy flow (total) during the operation of each cluster.

Cluster	Total demand (kWh)	Total generation (kWh)	Total supply (kWh)	Dem-Gen diff (%)	Status high gen (↑) Low gen (↓)	Action store (→) /supply (←)	Dem-sup diff (%)
1	9991.76	11 499.98	10 138.92	−14.27	↑	→	−0.74
2	13 778.75	12 604.07	13 714.17	9.18	↓	←	1.19
3	6151.09	9283.62	6237.81	−49.84	↑	→	−0.68
4	10 416.46	7421.78	10 496.87	29.26	↓	←	−0.05
5	9506.76	10 850.05	9493.94	−13.31	↑	→	0.85
6	8133.25	7315.82	7997.91	10.70	↓	←	1.37
7	9993.29	9484.11	9893.67	5.78	↓	←	1.71

that the generation level exceeds the demand, with the excess energy being supplied by the storage system. Furthermore, the demand-supply difference value offers insights into how effectively the system balances supply and generation operations. Negative values signify that the total supply falls short of the total demand, whereas positive values indicate that the total supply exceeds the total demand.

Given that the MILP model optimizes the problem across all seven clusters simultaneously, the sum of total demand and supply over these consecutive days equals zero. An energy balance constraint is imposed to limit the difference between demand and supply to not exceed 2%. This constraint demonstrates the robustness and validity of the proposed system. The energy supply patterns of RESs during

Table 10
Optimal energy/H_2 flow of RES and storage system during the each cluster.

Cluster	Grid		RES			Storage			
	Import (kWh)	Export (kWh)	PV (kWh)	WT (kWh)	mHydro (kWh)	BESS Cha. (kWh)	BESS Discha. (kWh)	H_2 Pro. (Kg)	H_2 Refu. (Kg)
1	0.00	0.00	2700.86	1188.60	3479.12	876.46	3067.99	47.69	63.58
2	0.00	0.00	1121.11	8715.37	2767.58	2498.38	2768.29	58.10	80.99
3	0.00	0.00	407.71	6869.03	2006.88	1892.40	359.89	75.41	39.65
4	0.00	0.00	3108.54	168.37	4144.86	747.36	2565.06	13.94	46.42
5	0.00	0.00	1528.79	6688.29	2632.97	3307.37	2545.54	31.84	19.04
6	0.00	0.00	3248.58	1964.03	2103.21	2286.23	2894.12	47.23	50.45
7	0.00	0.00	2096.90	4906.92	1598.91	1825.18	2780.59	48.37	61.22

Table 11
Percentage of optimal RES and storage system energy/H_2 supply including losses during each cluster.

Cluster	Grid		RES			Storage		Calculated total supply (%)	Losses (%)
	Import (%)	Export (%)	PV (%)	WT (%)	Mhydro (%)	Battery (%)	H_2 (%)		
1	0.00	0.00	26.64	11.72	34.31	19.65	6.30	98.62	1.38
2	0.00	0.00	8.17	63.55	20.18	−0.03	6.77	98.65	1.35
3	0.00	0.00	6.54	110.12	32.17	−26.45	−23.83	98.54	1.46
4	0.00	0.00	29.61	1.60	39.49	15.44	12.60	98.74	1.26
5	0.00	0.00	16.10	70.45	27.73	−9.56	−5.64	99.09	0.91
6	0.00	0.00	40.62	24.56	26.30	5.64	1.38	98.49	1.51
7	0.00	0.00	21.19	49.60	16.16	6.47	5.22	98.64	1.36

Table 12
SOE and SOH status comparison across the clusters' operational periods.

Cluster	Battery SOE (kWh)		Hydrogen (Kg)		Battery SOC (%)		Hydrogen SOH (%)		Satisfied the constraints
	Start	End	Start	End	Start	End	Start	End	
1	2490.00	498.00	48.47	32.92	100	20	100	68	Yes
2	498.00	501.67	32.92	9.96	20	20	68	21	Yes
3	501.67	2148.11	9.96	45.91	20	86	21	95	Yes
4	2148.11	527.15	45.91	13.25	86	21	95	27	Yes
5	527.15	1405.19	13.25	26.01	21	56	27	54	Yes
6	1405.19	1110.23	26.01	23.09	56	45	54	48	Yes
7	1110.23	577.89	23.09	9.97	45	23	48	21	Yes

operational periods are depicted in Fig. 13(c). Utilizing actual data from a specific location has revealed distinct generation patterns. Notably, there is an increased likelihood of WT generation when PV generation is low. Conversely, higher WT generation is typically accompanied by reduced PV output. Additionally, the figure illustrates that during periods of high generation from both PV and WT, the mHydro generation contributed a comparatively lower energy output. This analysis underscores the dynamic interplay between different RESs in response to varying operational conditions.

Table 10 details the energy supply from RESs over a seven-day operational period, presenting actual energy values inclusive of charging/production and discharging/refueling amounts. This table specifically quantifies hydrogen production and refueling in kilograms (kg). Furthermore, Table 11 provides a percentage breakdown of the energy supply. It includes the total calculated percentage of energy supply and associated losses incurred during operation. These losses stem from inefficiencies in charging/production and discharging/refueling processes, as well as from discrepancies in energy flow, including excesses and shortages. Notably, the aggregate of the calculated total energy supply and losses equals 100%, demonstrating the system's optimal energy flow performance. This data collectively offers a comprehensive view of the operational efficiency and energy management within the system.

Fig. 14(a) illustrates the charging and discharging periods, rates, and SOC of the BESS, while Fig. 14(b) displays the H_2 production and refueling periods, rates, and SOH of HSH. These figures indicate that the charging and discharging rates for both storage systems are maintained within predefined constraints. The SOC and SOH curves reveal that levels consistently remain within the 20% to 100% range under various conditions. Notably, a higher H_2 production rate is employed to utilize excess energy effectively. Conversely, the maximum H_2 refueling rate is set to match the peak H_2 demand, adhering to the constraint that H_2 storage must meet all H_2 demands.

To provide a more detailed understanding, Table 12 compiles comprehensive data on these aspects. This table allows for the observation of initial and final SOC and SOH values for each cluster. A key insight from the table is the operational strategy: during periods of high demand, the system fully discharges within acceptable limits, whereas during lower demand, it conservatively retains energy for future use. This demonstrates the system's effective management in balancing energy availability with demand requirements.

4.4. Techno-economic analysis

The cost analysis of transitioning from a grid-connected system to a MG for a community setting is based on local energy provider tariff rates. Various tariffs were considered to calculate the energy cost for each cluster. Utilizing Eq. (56), the cost of energy for the MG COE_{mg} was determined to be 0.1776 AUD/kWh. Subsequently, the MG's cost was calculated using this value. Table 13 details the total energy cost for each cluster under different tariff rates and MG conditions. Furthermore, Table 15 presents the percentage of optimized cost and carbon emission achieved by converting various tariffs to MG configurations and non-RES to RES-based transformation, respectively. Fig. 15(a) illustrates the percentage decrease in costs when the MG demand corresponds to various clusters.

The analysis indicates that the maximum financial benefit from transitioning to an MG is observed for communities previously under the

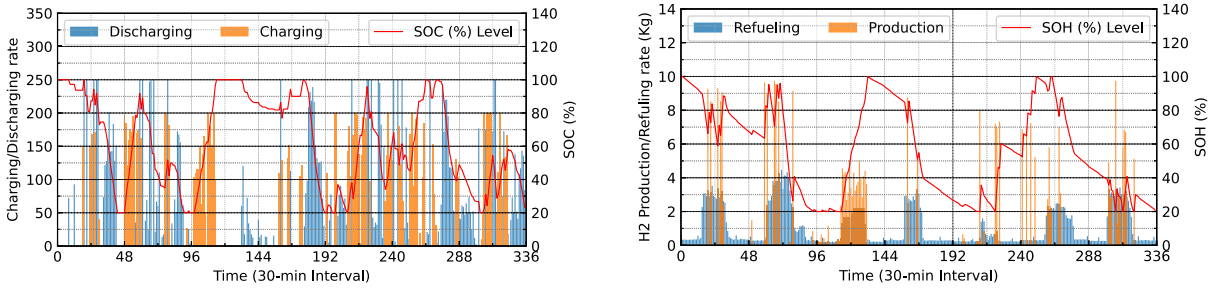

Fig. 14. Optimal scheduling of (a) BESS, charging and discharging rate, and SOC status and (b) H_2 storage, production, and refueling rate, and SOH status during the operation period.

Table 13
Energy cost of the existing system (considered as different energy communities) and the proposed MG system.

Cluster	Total demand (kWh)	GFT1 (AUD)	ToU (AUD)	GFT2 (AUD)	MG (AUD)
1	9991.76	3389.00	2498.97	2760.82	1774.93
2	13 778.75	4673.48	3347.48	3807.21	2447.65
3	6151.09	2086.33	1497.34	1699.61	1092.68
4	10 416.46	3533.05	2492.55	2878.17	1850.38
5	9506.76	3224.50	2280.07	2626.81	1688.78
6	8133.25	9660.43	6819.75	7869.79	1444.79
7	9993.29	3389.52	2481.42	2761.25	1775.21

Table 14
Carbon emission during each cluster's operation for different energy generation technology.

Cluster	Total demand (kWh)	Required carbon for different technology			
		GT (Kg)	Oil (Kg)	Coal (Kg)	PV+WT+mHydro (Kg)
1	9991.76	4995.88	6494.64	8992.58	179.56
2	13 778.75	6889.37	8956.19	12 400.87	119.30
3	6151.09	3075.55	3998.21	5535.98	65.55
4	10 416.46	5208.23	6770.70	9374.81	201.80
5	9506.76	4753.38	6179.39	8556.08	132.87
6	8133.25	4066.63	5286.62	7319.93	208.05
7	9993.29	4996.64	6495.64	8993.96	152.38

Table 15
Percentage of optimized cost and carbon emission of the MG concerning different energy technology.

Cluster	Optimized cost (%)			Optimized carbon emission (%)		
	GFT1 → MG	GToU →MG	GFT2 →MG	GT → MG	Oil → MG	Coal → MG
1	47.63	28.97	35.71	3.59	2.76	2.00
2	47.63	26.88	35.71	1.73	1.33	0.96
3	47.63	27.03	35.71	2.13	1.64	1.18
4	47.63	25.76	35.71	3.87	2.98	2.15
5	47.63	25.93	35.71	2.80	2.15	1.55
6	85.04	78.81	81.64	5.12	3.94	2.84
7	47.63	28.46	35.71	3.05	2.35	1.69

business low voltage ToU tariff, followed by the residential low voltage GFT-2, and then the business low voltage GFT-1 tariff. It is noted that for GFT, the percentage of cost and cost savings remain consistent across all seven clusters. However, for the ToU tariff, these figures vary, highlighting the impact of tariff structure on the financial benefits of adopting an MG system. This comprehensive analysis underscores the economic advantages of transitioning to an MG, particularly for specific tariff categories.

4.5. Carbon emission analysis

The carbon emission analysis for the MG, considering its grid-connected energy community context, is conducted by accounting for various energy generation sources. Recognizing that grid energy can originate from diverse sources such as gas turbines (GT), oil, or coal-based power plants, these technologies were employed to estimate the carbon emissions associated with utility grid energy. For the MG, carbon emissions were calculated based on its optimal capacity. Table 14 details the amount of carbon emissions, measured in kilograms, for different clusters and technologies. The comparative analysis of carbon emissions during the operation of the MG, post-transition from a traditional grid, is presented in Table 15. This table illustrates that the greatest reduction in carbon emissions is achieved when transitioning from a coal-based grid to a MG, followed by transitions from oil and GT-based systems, respectively. The data clearly indicates that adopting MG technology significantly lowers carbon emissions, especially when replacing energy sourced from high-emission technologies like coal. In addition, Fig. 15(b) illustrates the percentage decrease in carbon emission when the MG demand corresponds to various clusters. This transition not only supports more sustainable energy practices but also contributes to broader efforts to mitigate environmental impact.

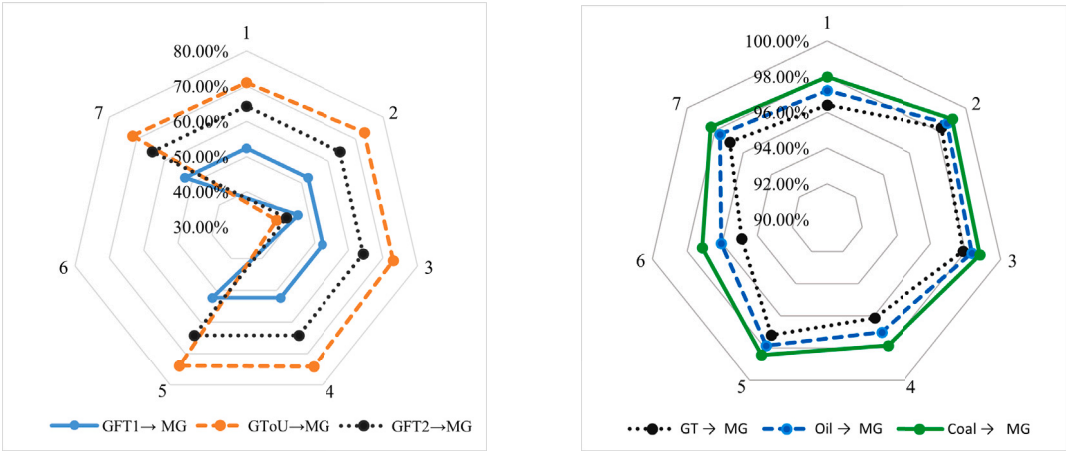

(a) (b)

Fig. 15. Percentage of (a) cost and (b) carbon emission after the transition of the MG at different clusters.

Table 16
Overall RES and storage system energy/H_2 flow.

PV	WT	mHydro	Initial BESS	Initial H_2
21.27%	47.37%	28.05%	1.60%	0.40%

Table 17
Comparison analysis of different transformation schemes.

Transformation technology		Cost savings	Carbon emission reduction
Tariff- based	GFT1→MG	47.03%	–
	GFT2→MG	57.73%	–
	GToU→MG	65.45%	–
Resource- based	GT→MG	–	96.82%
	Oil→MG	–	97.55%
	Coal→MG	–	98.23%

4.6. Overall analysis

In the preceding section, comprehensive analysis such as the energy flow, cost savings, and carbon emission impacts for each cluster is conducted within the proposed system. These clusters represent an aggregate of the entire year's energy generation and consumption data, offering a holistic view of the system's performance. Table 16 provides an overview of the total energy supply contributions from various RESs within the MG. This data indicates that the WT system is the predominant energy supplier to the MG, followed by mHydro, and finally the PV system. The analysis also takes into account the initial SOC and SOH of the BESS and H_2 storage, and their contributions are delineated in the table. This comprehensive analysis, encompassing the entire year, allows for a detailed understanding of the proposed system's energy dynamics, highlighting the significant contributions of various RESs and storage systems to the overall energy matrix. It underscores the effectiveness of integrating multiple energy sources and storage solutions in enhancing the efficiency and sustainability of the MG.

However, the cost analysis and carbon emission status for the overall system operation are detailed in Table 17. The table provide valuable insights into the economic and environmental benefits of implementing the proposed MG system. The table reveals that significant cost savings can be achieved, particularly among business users within the community. For residential users, the implementation of the MG system is projected to result in substantial energy cost savings, amounting to approximately 53.27%. This indicates a notable financial benefit for residents, highlighting the cost-effectiveness of the MG system. Regarding carbon emissions, the results demonstrate that transitioning from a coal-based grid to an MG system offers the most substantial reduction in carbon emissions, with a remarkable decrease of about 98.23%. This drastic reduction underscores the MG's effectiveness in significantly lowering the carbon footprint of energy consumption, particularly when replacing coal-based energy sources. However, the statistical analysis of cost reduction and carbon emission reduction are presented in Figs. 16(a) and 16(b), respectively.

5. Discussion

The discussion revolves around optimizing the capacity of RES and storage systems. According to the findings, the optimization process utilizes a dataset clustered into seven groups to ensure a reliable and cost-effective energy setup for a community. The results indicate that the capacities of RES and storage systems are guided by the values of α, which influence the optimization algorithm, favoring higher capacities for systems with lower α values to reduce costs. Despite its high α, HSH is constrained to ensure its cost does not excessively affect the capacity determination. Moreover, an increased capacity in BESS is targeted to enhance system reliability, ensuring sufficient energy supply even when RES generation is low.

The optimal energy flow analysis reveals the energy supply and demand patterns across seven clusters, helping to validate the system's efficiency and reliability through sensitivity analysis. Notably, discrepancies between demand and supply provide insights into the system's balance, indicating situations where energy is either stored due to surplus or supplied from storage due to shortages. Key operational details include the energy supply patterns of RESs, such as WT and PV, which show a dynamic interplay depending on operational conditions. The system's ability to manage energy efficiently is also demonstrated by the energy balance constraint, ensuring that the difference between demand and supply does not exceed 2%. Additionally, the system's operational efficiency is reflected in how it manages charging and discharging activities within the BESS and HSH, with storage levels maintained within optimal ranges to match energy supply and demand effectively.

Table 13 specifically examines the costs associated with existing energy systems—categorized under GFT1, GFT2, and ToU—compared to a proposed MG system. Notably, the proposed MG system presents lower costs in nearly all instances when compared to the flat tariffs and performs competitively under the ToU pricing. Moreover, Table 14 expands on the environmental aspect by detailing the carbon emissions from different energy generation technologies. The data clearly show that traditional technologies emit substantially more carbon than

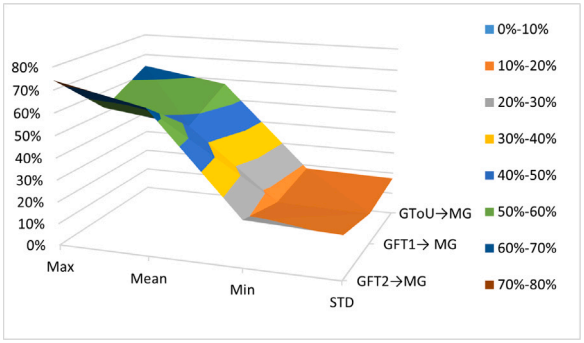

(a) Percentage of cost reduction in different clusters.

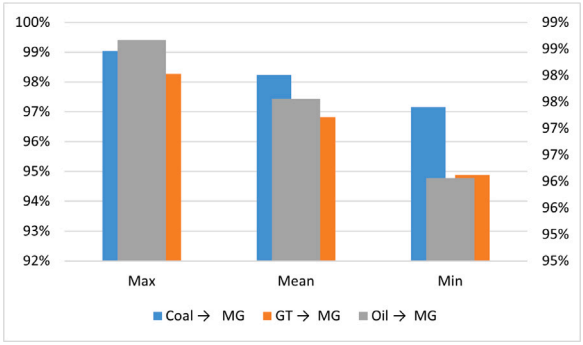

(b) Percentage of carbon emission reduction in different clusters.

Fig. 16. Statistical analysis of the (a) percentage of cost reduction in different transition schemes and (b) percentage of carbon emission reduction in several tariff settings during multiple clusters.

renewable technologies. Furthermore, Table 15 illustrates the potential for cost and emission reductions when switching from traditional systems to an MG setup. It presents the optimized conditions for cost and carbon emissions, demonstrating significant improvements in both areas across all clusters. These findings highlight the cost effectiveness and environmental advantages of transitioning the traditional energy system to RES-based MG.

Tables 16 and 17 illustrate the overall benefits of transitioning the existing energy system to RES-based MG. Table 16 shows that in an optimal renewable energy setup under the considered energy community, WT, and mhydro are the most significant energy contributors, highlighting their reliability and availability. Table 17 reveals that switching from traditional tariff-based energy systems to MG results in significant cost savings, particularly when moving from ToU tariffs. Moreover, transitioning from fossil fuel-based systems (GT, Oil, Coal) to MG drastically reduces carbon emissions. These findings collectively demonstrate the dual benefits of the MG system: achieving considerable cost savings while also substantially reducing carbon emissions, thereby contributing to both economic and environmental sustainability.

6. Conclusion

In this study, a hybrid MLCP-based bi-level PSO-MILP optimization algorithm is developed to design and enhance the performance of an MG within an energy community. The proposed system integrates the MLCP approach to clustering and profiling the data by utilizing historical meteorological data, RES parameters, and the community's energy demand and incorporating emerging technologies like FCEV demand. This approach also uniquely combines two advanced optimization models to simultaneously determine the optimal capacity of RESs and storage systems through the optimal operation. The system's effectiveness was assessed through metrics such as optimal energy flow, cost savings, and carbon emission reduction. The results indicate significant improvements, with the system operating optimally in seven clustered scenarios. Notably, the cost of running the MG could be reduced by up to 65.45% compared to current energy expenses and carbon emissions potentially decreased by as much as 98.23% when transitioning from a coal-based grid. Similarly, transforming GFT1-based and GFT2-based LV grid systems to MG led to cost reductions of 47.03% and 57.73%, respectively. Additionally, carbon emissions were decreased by 96.82% for the transition from GT to MG and by 97.55% for the transition from oil to MG. In conclusion, the proposed AI-integrated system markedly enhances MG performance, and future updates will focus on incorporating advanced AI algorithms for day-ahead operations, shifting from traditional to intelligent grid systems.

CRediT authorship contribution statement

Md Morshed Alam: Writing – original draft, Software, Methodology, Formal analysis, Data curation, Conceptualization. **M.J. Hossain:** Writing – review & editing, Validation, Supervision. **Muhammad Ahsan Zamee:** Writing – review & editing, Validation, Methodology, Investigation. **Ahmed Al-Durra:** Writing – review & editing, Validation, Supervision.

Declaration of competing interest

The authors declare that they have no known competing financial interests or personal relationships that could have appeared to influence the work reported in this paper.

Data availability

The data that has been used is confidential.

References

[1] Zhou J, Xu Z. Optimal sizing design and integrated cost-benefit assessment of stand-alone microgrid system with different energy storage employing chameleon swarm algorithm: A rural case in Northeast China. Renew Energy 2023;202:1110–37.
[2] Essayeh C, Morstyn T. Optimal sizing for microgrids integrating distributed flexibility with the perth west smart city as a case study. Appl Energy 2023;336(120846):120846.
[3] Medghalchi Z, Taylan O. A novel hybrid optimization framework for sizing renewable energy systems integrated with energy storage systems with solar photovoltaics, wind, battery and electrolyzer-fuel cell. Energy Convers Manag 2023;294(117594):117594.
[4] Jiang S, Wen S, Zhu M, Huang Y, Ye H. Scenario-transformation-based optimal sizing of hybrid hydrogen-battery storage for multi-timescale islanded microgrids. IEEE Trans Sustain Energy 2023;14(3):1784–95.
[5] Akter H, Howlader HOR, Nakadomari A, Islam MR, Saber AY, Senjyu T. A short assessment of renewable energy for optimal sizing of 100% renewable energy based microgrids in remote islands of developing countries: A case study in Bangladesh. Energies 2022;15(3):1084.
[6] Bin L, Shahzad M, Javed H, Muqeet HA, Akhter MN, Liaqat R, et al. Scheduling and sizing of campus microgrid considering demand response and economic analysis. Sensors (Basel) 2022;22(16):6150.
[7] Nair A, Kumar AG, Lavanya MC, Katyal R, Menicucci A. Optimal sizing of hybrid PV-BESS based residential microgrid for rural electrification. In: 2022 IEEE students conference on engineering and systems (SCES). IEEE; 2022.
[8] Garip S, Ozdemir S. Optimization of PV and battery energy storage size in grid-connected microgrid. Appl Sci (Basel) 2022;12(16):8247.
[9] Guru N, Nayak MR, Barisal AK, Patnaik S. Optimal sizing of battery energy storage in solar microgrid considering peak load shaving. Int J Ambient Energy 2023;44(1):2362–71.
[10] Borkowski D, Oramus P, Brzezinka M. Battery energy storage system for grid-connected photovoltaic farm – energy management strategy and sizing optimization algorithm. J Energy Storage 2023;72(108201):108201.

[11] Khezri R, Mahmoudi A, Haque MH. Impact of optimal sizing of wind turbine and battery energy storage for a grid-connected household with/without an electric vehicle. IEEE Trans Ind Inf 2022;18(9):5838–48.
[12] May Alvarez JA, Zurbriggen IG, Paz F, Ordonez M. Microgrids multiobjective design optimization for critical loads. IEEE Trans Smart Grid 2023;14(1):17–28.
[13] Heydari A, Nezhad MM, Keynia F, Fekih A, Shahsavari-Pour N, Garcia DA, et al. A combined multi-objective intelligent optimization approach considering techno-economic and reliability factors for hybrid-renewable microgrid systems. J Clean Prod 2023;383(135249):135249.
[14] Hakimi SM, Hasankhani A, Shafie-khah M, Lotfi M, Catalão JPS. Optimal sizing of renewable energy systems in a microgrid considering electricity market interaction and reliability analysis. Electric Power Syst Res 2022;203(107678):107678.
[15] Khawaja Y, Qiqieh I, Alzubi J, Alzubi O, Allahham A, Giaouris D. Design of cost-based sizing and energy management framework for standalone microgrid using reinforcement learning. Sol Energy 2023;251:249–60.
[16] Bandyopadhyay S, Mouli GRC, Qin Z, Elizondo LR, Bauer P. Techno-economical model based optimal sizing of PV-battery systems for microgrids. IEEE Trans Sustain Energy 2020;11(3):1657–68.
[17] Khezri R, Mahmoudi A, Whaley D. Optimal sizing and comparative analysis of rooftop PV and battery for grid-connected households with all-electric and gas-electricity utility. Energy (Oxf) 2022;251(123876):123876.
[18] Bacha B, Ghodbane H, Dahmani H, Betka A, Toumi A, Chouder A. Optimal sizing of a hybrid microgrid system using solar, wind, diesel, and battery energy storage to alleviate energy poverty in a rural area of biskra, Algeria. J Energy Storage 2024;84(110651):110651.
[19] Yaldız A, Gökçek T, Şengör İ, Erdinç O. Optimal sizing and economic analysis of photovoltaic distributed generation with battery energy storage system considering peer-to-peer energy trading. Sustain Energy Grids Netw 2021;28(100540):100540.
[20] Bhamidi L, Sivasubramani S. Optimal sizing of smart home renewable energy resources and battery under prosumer-based energy management. IEEE Syst J 2021;15(1):105–13.
[21] Tostado-Véliz M, Icaza-Alvarez D, Jurado F. A novel methodology for optimal sizing photovoltaic-battery systems in smart homes considering grid outages and demand response. Renew Energy 2021;170:884–96.
[22] Morales R, Marín LG, Roje T, Caquilpan V, Sáez D, Nuñez A. Microgrid planning based on computational intelligence methods for rural communities: A case study in the josé painecura mapuche community, chile. Expert Syst Appl 2024;235(121179):121179.
[23] Tayyab Q, Qani NA, Elkholy MH, Ahmed S, Yona A, Senjyu T. Techno-economic configuration of an optimized resident microgrid: A case study for afghanistan. Renew Energy 2024;224(120097):120097.
[24] Korjani S, Casu F, Damiano A, Pilloni V, Serpi A. An online energy management tool for sizing integrated PV-BESS systems for residential prosumers. Appl Energy 2022;313(118765):118765.
[25] Yan C, Zou Y, Wu Z, Maleki A. Effect of various design configurations and operating conditions for optimization of a wind/solar/hydrogen/fuel cell hybrid microgrid system by a bio-inspired algorithm. Int J Hydrogen Energy 2024;60:378–91.
[26] Mewafy A, Ismael I, Kaddah SS, Hu W, Chen Z, Abulanwar S. Optimal design of multiuse hybrid microgrids power by green hydrogen–ammonia. Renew Sustain Energy Rev 2024;192(114174):114174.
[27] Akulker H, Aydin E. Equipment selection for coupling a microgrid with a power-to-gas system in the context of optimal design and operation. Comput Chem Eng 2024;181(108512):108512.
[28] Gholami M, Muyeen SM, Lin S. Optimizing microgrid efficiency: Coordinating commercial and residential demand patterns with shared battery energy storage. J Energy Storage 2024;88(111485):111485.
[29] Tatar SM, Aydin E. Design and operation of renewable energy microgrids under uncertainty towards green deal and minimum carbon emissions. SSRN Electron J 2023.
[30] Vaka SSKR, Matam SK. Prediction-based optimal sizing of battery energy storage systems in PV integrated microgrids for electricity bill minimization. J Inst Eng (India) Ser B 2022;103(5):1733–45.
[31] Alam MM, Bin Mofidul R, Jang YM. Community energy storage system: Deep learning based optimal energy management solution for residential community. J Energy Storage 2023;64(107100):107100.
[32] Tabandeh A, Hossain MJ, Li L. Integrated multi-stage and multi-zone distribution network expansion planning with renewable energy sources and hydrogen refuelling stations for fuel cell vehicles. Appl Energy 2022;319(119242):119242.
[33] CO2 emissions due to electricity generation, https://www.rensmart.com/Calculators/KWH-to-CO2, Accessed: 2023-11-27.
[34] Graham Paul, Hayward Jenny, Foster James, Havas Lisa. GenCost 2021-22, https://www.csiro.au/-/media/News-releases/2022/GenCost-2022/GenCost2021-22Final_20220708.pdf, Accessed: 2023-27-11 (Jul. 2022).
[35] Hydro-Electric Corporation, Pumped hydro cost modelling, https://www.aemo.com.au/-/media/Files/Electricity/NEM/Planning_and_Forecasting/Inputs-Assumptions-Methodologies/2019/Report-Pumped-Hydro-Cost-Modelling.pdf, Accessed: 2023-27-11.